Exploring the Chemistry of Re^{I}: Physical and Theoretical Investigations

by

Philip D. Bulsink

Thesis submitted to the
Faculty of Graduate and Postdoctoral Studies
In partial fulfilment of the requirements
For the degree of

Master of Science
In
Chemistry

Ottawa-Carleton Chemistry Institute
University of Ottawa

Supervisors: *Professors Darrin Richeson & Tom Woo*

Abstract

The development of Rhenium I photocatalysts has been pursued since Lehn first showed the excellent performance of the Re^{I} bipyridine tricarbonyl catalyst. Since then, development has modified the organic ligand to demonstrate continued or improved activity with other α-diimine bidentate geometries. Geometry has been limited to κ^2 motifs, with *fac*-$(CO)_3$ and axial halides. This work will demonstrate the synthesis, characterization, and testing of a new $\kappa^3(L_3)-Re^1(CO)_2X$ (X = Cl, Br, CN, OTf) family of compounds for CO_2 reduction, as well as computational investigations into the mechanism of the reduction of CO_2 to CO and other species.

Acknowledgements

I'm thankful for the assistance of my supervisors Dr. Darrin Richeson and Dr. Tom Woo, in guiding this research, providing suggestions and assistance, and for help with editing of this thesis and other papers and projects.

Thanks to the members of the Richeson and Woo research groups, both past and present, for the assistance provided and for making the time spent researching and writing this thesis enjoyable. Thanks as well to Frank and Sean in the Brusso lab, for their help with their spectroscopic characterization equipment (IR, UV-Vis, and Fluorescence). Thanks to Jake and the Gambarotta laboratory for use of their GC, Rola and the Detellier lab for the assistance with the TGA, and to the Sciano Lab, especially Janice, Charles, and Deni, for their assistance in use of their photolysis equipment.

I'd like to thank Dr. Ilia Korobkov for his work measuring and solving the x-ray crystal structures of the compounds discussed. He assisted with some paper writing as well.

Finally, I'd like to thank my wife Leanne and my parents for their unending support, and understanding when I came home frustrated or exhausted from a day in the lab.

Contents

List of Tables

List of Figures

List of Schemes

Chapter 1

Introduction

Common distinctions split most chemical compounds into one of two categories: organic and inorganic. Organic molecules contain carbon and hydrogen, with or without additional nitrogen, oxygen, phosphorus, sulphur, and the halides. Inorganic chemistry is, therefore, considered to be the remainder of the molecules possible. While they may include come aspect of organic chemistry (especially in organometallic molecules), the main structural motif or reactive center is a non-organic feature. These inorganic compounds can range from compounds such as lithium or Grignard reagents with significant organic influence, to metallic alloys or mineral compounds. With such a wide range of possibilities, inorganic chemistry has many facets. A widely active research area is the development and testing of transition metal complexes for catalytic, photo-physical, biochemical or manufacturing uses.

1.1 Photochemistry & Catalysis

A report of the first synthesized organometallic complex was published by Zeise in 1831.[1] To form what is now known as Zeise's salt, $K[PtCl_3(C_2H_4)] \cdot H_2O$, he mixed platinum

chloride with ethanol, followed by a reaction with potassium chloride.[2] After some controversy to the composition of this, it was confirmed by Griess and Martius,[3] and later expanded upon by Birnbaum.[4]

The field of organometallics was expanded greatly by Frankland,[2] and many of his complexes were catalytically active. Further development of this new type of chemistry quickly led to useful catalysts for the conversion of petroleum products and other chemistries, using nearly all of the transition metals. These catalysts take all forms, from simple olefin and halide compounds to multi-metallic complexes with large organic ligands.

Some of the most significant organometallic catalysts since the late 1990s have been the development of earth metal pincer complexes to replace noble metal or early transition metal catalysts, which are often more toxic or expensive to produce. Brookhart and Gibson published a series of papers[5–8] on the use of iron and cobalt with bis(imino)pyridine ligands to perform ethylene polymerization at rates exceeding those of similar noble metal complexes and metallocenes.[9] The role of the ligand in the mechanism is still up for debate, but many modified systems have been synthesized and tested since the first work was published.[10]

Many of these types of pincer complexes are photochemically active. In transition metal complexes, the interaction between the metal atom(s) and the ligands can cause significant electron mobility upon the absorption of incident photons. The metal atom's d orbitals typically lie at or near the Highest Occupied Molecular Orbital (HOMO) energy, while the ligands often have low energy anti-bonding orbitals (π^*) at the Lowest Unoccupied Molecular Orbital (LUMO) levels. When a photon is absorbed and is promoted from the ground state to the excited state, that state is spatially removed from the metal centre, this motion of the electron is labelled a Metal-Ligand Charge Transfer

(MLCT). Formally, the metal atom is oxidized by the photons, this oxidation allows for redox reactivity at the metal centre for as long as the electron remains removed to the ligand. Relaxation (through photon emission via fluorescence or phosphorescence, or via vibrational or other motion processes) can return the electron to the metal to reform the ground electronic state.

1.2 Rhenium

Rhenium compounds in particular are known to have a broad range of applications. Their use in catalysis has been explored, covering olefin hydrogenation,[11] epoxidation (with chiral selectivity),[12] and in a host of organic bond formation reactions[13] (Friedel-Crafts acylation and alkylation,[14–16] nucleophilic addition,[17,18] carbon-carbon coupling,[19,20] as well as other heteroatom-carbon bond formation[21–25]). Rhenium has also been used in radiopharmaceutical applications, due to the availability of moderately radioactive isotopes.[26,27] These compounds exhibit other interesting fundamental photophysical properties as well.[28]

Since the mid-1970s, complexes containing the α-diimine Re^{I} tricarbonyl core have attracted a great deal of attention due to their attractive photochemical properties. The pseudo-octahedral *fac*-$[L_2Re(CO)_3X]$ and *fac*-$[L_2(L')Re(CO)_3]^+$ complexes have been the dominant species.[29–39] A large family of compounds with these formulations have been accessed by the addition of chelating diimine σ-donor ligands to $[Re(CO)_5X]$ with the quantitative replacement of two *cis* carbonyls in the Re^{I} starting material.[29,40–48] Significantly, these reactions form only bidentate coordinated ligands with *facial* tricarbonyl isomers as products even when a potentially tridentate σ-donor, such as bis(imino)pyridine or 2,2':6',2"-terpyridine. are employed in the reaction (see Figure 1.1).[49–52]

These robust species have been examined for potential applications in organic light-

emitting diodes (OLEDs),[53,54] chemosensors and biotechnology probes,[55–59] fluorescence microscopy imaging of cells,[55,60–63] as chemotherapy agents,[64] in the formation of macromolecules,[65] and the photochemical reduction of CO_2 to CO.[66–70] Among the key photophysical features of these α-diimine Re^I compounds is the electron transfer capability of this system and the interplay between the Re center and the well-known non-innocent redox activity of the ligands.[71,72]

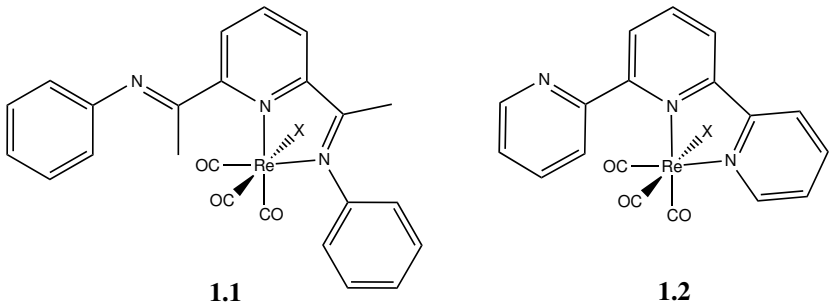

1.1 **1.2**

X = Cl, Br, I

Figure 1.1 Two common *fac*-[$L_2Re(CO)_3X$] complexes with terdentate σ-donor ligands: L = bis(imino)pyridine (**1.1**) and 2,2':6',2"-terpyridine (**1.2**).

Further development of this chemistry has been restricted by the limited structural and electronic variability of the common pseudo-octahedral *fac*-[$L_2ReX(CO)_3$] (L_2 = α-diimine) products. While these systems continue to receive considerable attention, studies detailing the coordination chemistry of the meridionally-coordinated tridentate triimine Re^I dicarbonyl core are quite limited.[73] For example, while κ^3(terpy)$Re(CO)_2Cl$ was initially reported in 1988,[74] closer analysis of the reported analytical data (including ^{1}H NMR) indicate that this compound is more likely κ^2L$Re(CO)_3Cl$. A more recent report for this compound provides spectroscopic details of this species as well as the preliminary report for the generation of $[\kappa^3(terpy)Re(CO)_2L']^+$ cations (L = PPh_3, PEt_3, NC_5H_5, and $NCCH_3$).[75] Finally, the ^{1}H NMR data for κ^3(terpy)$Re(CO)_2Br$ has been reported[51] but accompanied no other characterization.

In order to fully exploit the potential of this versatile family of compounds, the limits imposed by the bidentate coordination need to be addressed. Furthermore, it would appear that, on the basis of the tridentate ligands that have been investigated, the concerted effort to produce the tridentate species has been essentially unsuccessful, or requiring harsh conditions.[52]

1.3 CO_2 Reduction Chemistry

Recent years have seen an increase in the concentration of CO_2 in the atmosphere as a product of combustion of oil, gas and coal in the industry and transportation sectors.[76] This is of significant concern due to the greenhouse gas properties of CO_2.[77,78] Attempts to reduce emissions proceed by various pathways, including the utilization of renewable resources such as wind and solar for energy production;[79] development of more fuel and energy efficient processes; and attempts to capture CO_2 from industrial exhaust streams.[80–82] It can then be stored in underground depositories, or used as a feedstock in the production of simple molecules or fuels.[83–85] Due to it being the final product in combustion and its high thermodynamic stability, the reduction of CO_2 is an energy-intensive task.[86,87] While plant life naturally performs CO_2 transformation via photosynthesis, no artificial means have proven to be robust and scalable enough for the task in large scale.[88]

The development of catalysts for 'artificial photosynthesis' has explored various means, including utilizing metal electrodes,[89] electrocatalytic semiconductors (such as TiO_2, ZnS, CdS, or As or S doped Ag),[90,91] and organometallic species of Co, Ni, Mn, and Fe (particularly porphyrin complexes).[92–102] These typically require the addition of electrons, and current trends look to solar powered electricity production for a 'green' CO_2 reduction platform.[103–105]

Alternate solutions involves the use of photoredox catalysts, including α-diimino complexes of Re^{I}, Ru^{II}, Os^{II}, and Ir^{III}.[66,106–116] In recent years, the popularity of these α-diimino compounds has increased, owing to their unique MLCT excited states and easily tunable photophysical properties. Of these complexes, Re^{I} based catalysts are of particular interest. Whether acting as a mono-metallic photocatalyst, or with Ru in multi-metallic complexes, the high quantum yield (up to Φ=0.59)[117,118] and exclusive selectivity to production of CO is unparalleled in these catalysts.[119,120] Research focus has turned to tuning photophysical properties for increased use of photons in the visible spectrum (particularly lower energy) and modification of the ligand framework for increased turnover numbers and frequencies.[87,119,121–123]

1.4 Objectives

Attracted by the challenge of synthesizing Re^{I} terdentate compounds, the objectives were to synthesize, crystallographically authenticate, and investigate the photophysical properties of low-valent rhenium pincer complexes displaying an N,N',N"-chelated terpyridine array.

Complexes of 2,2':6',2"-terpyridine (terpy) are of interest due to the conceptual relationship to established bis(imino)pyridine compounds.[124,125] This thesis will be a discussion of the development of chemistry of Re^{I} complexes, their characterization, and comparison of structural and photo-physical properties to computed values.

This thesis will focus on the synthesis and testing of a novel Re^{I} catalyst attempting to improve on those points. It will also provide a more detailed examination at specifics of the mechanisms proposed for current Re^{I} diimine catalysts, and propose new geometries for prior mechanistic steps based on experimental, computational, and literature review work.

Chapter 2

New Coordination Geometries for Re^{I}

2.1 Introduction

Re^{I} compounds have been typically bidentate (κ^2) compounds, even when using a potentially terdentate (κ^3) ligand such as bis(imino)pyridine or terpyridine (refer to Figure 1.1). The chemistry of this rhenium α-diimino complex has been extensively investigated, with over 1700 references appearing in a SciFinder structure search for that metal-ligand motif.[126] The ejection of an additional carbonyl and the chelation of the pendant arm of the ligand was attempted to extend the conjugated π system of the ligand and its interaction with the metal centre. This was first demonstrated by prior work in our group for the bis(imino)pyridine ligand.[73] This section will demonstrate the expansion of the possible rhenium(I) pincer complex geometries by synthesizing and characterizing a series of terdentate complexes with the 2,2':6'2"-terpyridine ligand.

2.2 Synthesis of Bidentate and Terdentate Re$^{\mathbf{I}}$ Complexes

Similar to the prior work, synthesis began with the production of the bidentate complex κ^2(terpy)Re(CO)$_3$X (X = Cl, Br) by coordination of 2,2':6',2"-terpyridine with a Re(CO)$_5$X starting material in dry toluene at reflux for 4 hours, as shown in Scheme 2.1. A bright yellow powder precipitated from solution and was collected by filtration, washed with cold hexanes, and dried *in vacuo* to a good yield of **2.1** and **2.3** respectively.[i] These bidentate compounds were characterized fully and used without further purification to produce κ^3(terpy)Re(CO)$_2$X (X = Cl, Br) via thermolysis, as well as for anion exchange reactions.

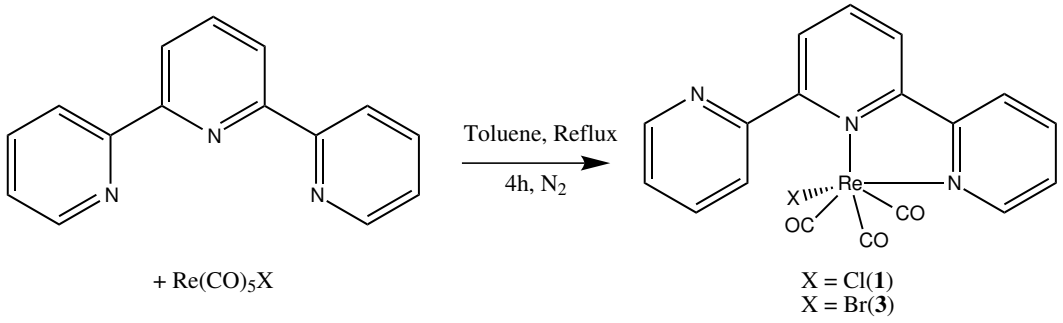

Scheme 2.1 Synthesis of **2.1** and **2.3** from Re(CO)$_5$X and 2,2':6',2"-terpyridine.

Conversion of compounds **2.1** and **2.3** to the κ^3 moiety required the release of CO and the subsequent coordination of the free pendant arm. Prior work had identified the thermal lability of the carbonyl, based on a method first described by Buckingham with a osmium complexes.[127] In this method, a ceramic sample boat was placed in a tube furnace at elevated temperature, under a flowing atmosphere of N_2. After some time, the sample is removed and collected at nearly quantitative yield. Determination of

[i]Experimental details for all compounds can be seen in Appendix A Experimental Procedures

2.3.2 Structure Analysis with X-Ray Crystallography and DFT

Single crystal analysis by x-ray crystallography yielded good structures of compounds **2.1**, **2.2**, **2.3**, **2.5**, and **2.8**. These are the first reported crystal structures of the κ^3 terdentate Re^I compounds. A number of structural characteristics are common between the various bidentate or terdentate complexes. Much analysis has been done on the structures of bidentate complexes in literature[130–132] the notable characteristic within terpyridine compounds is the rotation of the pendant arm, pushing the nitrogen atom away from the plane of the metal-ligand bonds by approximately 100°. Cell parameters and other collection data for compounds **2.1**, **2.3**, **2.5**, and **2.7** are located in Table 2.1.

Table 2.1 Crystal data and structure refinement for compounds **2.1**, **2.3**, and **2.5**

Compound	**2.1**	**2.3**	**2.5**
Empirical formula	$C_{19}H_{11}N_3O_3ReCl$	$C_{19}H_{11}N_3O_3ReBr$	$C_{20}H_{11}N_4O_3Re$
Formula weight (g/mol)	538.96	583.41	530.04
Temperature (K)	200	200	200
Wavelength (Å)	0.71073	0.71073	0.71073
Crystal System	Triclinic	Monoclinic	Triclinic
Space Group	P-1	C2/c	P-1
a (Å)	9.8736(4)	31.1537(7)	9.9196(9)
b (Å)	14.8202(4)	7.1176(2)	14.9902(14)
c (Å)	16.3472(4)	16.8519(4)	16.5187(15)
α (deg)	69.2890(10)	90.000	68.363(2)
β (deg)	80.801(2)	111.0230(10)	80.929(2)
γ (deg)	79.836(2)	90.000	79.975(2)
Volume ($Å^3$)	2190.00(12)	3488.00	2236.6(4)
Z, r (calc) (Mg/m^3)	2, 1.997	8, 2.222	2, 1.927
Absorption coefficient (mm^{-1})	6.063	9.282	5.821
Absorption correction	Semi-empirical from equivalents		
Final R indices [I≥2σ(I)]	R1 = 0.0397, wR2 = 0.0839	R1 = 0.0232, wR2 = 0.0614	R1 = 0.0390, wR2 = 0.0921
R indices (all data)	R1 = 0.0604, wR2 = 0.0951	R1 = 0.0285, wR2 = 0.0642	R1 = 0.0500, wR2 = 0.0961

In addition, the structures of all species were geometry optimized at the first principles DFT level, with the B3LYP exchange-correlation functional[133,134] using the Gaussian 09

quantum chemistry package.[135] The LanL2DZ basis set/effective core potential was used on Re,[136] and the all-electron TZVP basis set for the remaining lighter atoms.[137] These are popular basis set and functional choices for computational chemistry, owing to their reasonable accuracy with decent computational speed,[138] although they are not without their faults.[139] Frequency analysis of all structures was used to confirm the nature of the stationary points. Solvent effects were computed when necessary using the integral equation formalism variant of the Polarizable Continuum Model (PCM) for solvation within Gaussian 09.[140,141]The results of these calculations are compared to the x-ray crystallography data in Tables 2.3 to 2.7.

The crystal structure of **2.3** had a higher symmetry than the other samples. Details on the exact methods used for structure elucidation are available in section A.3. All of the structures found are of high quality. The structures of **2.1**, **2.3**, and **2.5** can be seen in Figure 2.7. More views of these structures can be seen in Appendix section A.3. Crystals suitable for x-ray analysis were unable to be collected from compound **2.7**.

Selected bond lengths, bond angles, and torsion angles are listed in Table 2.3, Table 2.4 and Table 2.5 for products **2.1**, **2.3**, and **2.5** respectively. The experimental results agree closely with the computed values for all samples. The structures can be seen in Figure 2.7a, Figure 2.7b and Figure 2.7c, and more views of these structures can be seen in Appendix B, X-ray Crystal Structures.

The Re^I centre in the pseudo-octahedral complex is supported by a planar, pincer coordinated ligand defined by the terminal and central pyridyl group of the terpyridine. One of the carbonyl groups lies in this plane trans to the central pyridyl group, while the remaining carbonyl groups and the anionic group or other complexed species lie on an approximately perpendicular plane to the ligand. Bond angles around the Re centre show a significant deviation of up to 15° from the ideal octahedral geometry for all samples

ture solved to the two isomers, critical analysis would suggest that this molecule does not violate the axial position pattern laid out above. The computed structures energies in Table 2.2 show a favouring of the axial position by 12-16 kcal/mol in the gas phase and by PCM in a simulated acetonitrile solvent.

Selected bond lengths, bond angles, and torsions are listed in Table 2.3, Table 2.4 and Table 2.5 for products **2.1**, **2.3**, and **2.5** respectively.

Table 2.3 Selected Distances, Angles, and Torsions for **2.1**.

Bond	Distance (Å)	
	Experimental	Calculated
Re(1)-C(16)	1.89(1)	1.91
Re(1)-C(17)	1.934(8)	1.94
Re(1)-C(18)	1.90(1)	1.92
Re(1)-N(1)	2.162(6)	2.20
Re(1)-N(2)	2.236(9)	2.29
Re(1)-Cl(1)	2.496(2)	2.52
C(16)-O(1)	1.16(1)	1.15
C(17)-O(2)	1.12(1)	1.15
C(18)-O(3)	1.15(1)	1.16
Angle	Degrees (°)	
	Experimental	Calculated
C(16)-Re(1)-C(17)	87.6(4)	86.9
C(16)-Re(1)-C(18)	88.3(4)	90.6
C(17)-Re(1)-C(18)	87.3(4)	89.6
C(16)-Re(1)-N(1)	96.4(3)	96.2
C(17)-Re(1)-N(1)	174.9(3)	175.6
C(18)-Re(1)-N(1)	95.9(3)	93.5
C(16)-Re(1)-N(2)	169.3(3)	170.4
C(17)-Re(1)-N(2)	101.1(3)	102.8
C(18)-Re(1)-N(2)	98.3(3)	89.4
N(2)-Re(1)-N(1)	74.5(3)	74.1
C(16)-Re(1)-Cl(1)	91.7(3)	91.4
C(17)-Re(1)-Cl(1)	91.7(3)	94.8
C(18)-Re(1)-Cl(1)	179.9(3)	175.3
N(1)-Re(1)-Cl(1)	84.0(2)	82.0
N(2)-Re(1)-Cl(1)	81.6(2)	87.8
O(1)-C(16)-Re(1)	179.6(9)	178.2
O(2)-C(17)-Re(1)	176.0(8)	176.9
O(3)-C(18)-Re(1)	177.3(9)	179.3
Torsion	Degrees (°)	
	Experimental	Calculated
N(1)-C(5)-C(6)-N(2)	16(1)	15
N(2)-C(10)-C(11)-N(3)	41(1)	139

Table 2.4 Selected Distances, Angles, and Torsions for **2.3**.

Bond	Distance (Å)	
	Experimental	Calculated
Re(1)-C(16)	1.911(3)	1.92
Re(1)-C(17)	1.890(3)	1.92
Re(1)-C(18)	1.921(4)	1.94
Re(1)-N(1)	2.173(3)	2.20
Re(1)-N(2)	2.232(2)	2.29
Re(1)-Br(1)	2.6410(4)	2.68
C(16)-O(1)	1.150(4)	1.15
C(17)-O(2)	1.157(4)	1.15
C(18)-O(3)	1.155(5)	1.16
Angle	Degrees (°)	
	Experimental	Calculated
C(16)-Re(1)-C(17)	89.1(1)	90.8
C(16)-Re(1)-C(18)	85.9(1)	86.8
C(16)-Re(1)-N(1)	97.9(1)	96.0
C(17)-Re(1)-N(1)	92.5(1)	93.6
C(18)-Re(1)-N(1)	175.4(1)	175.6
C(16)-Re(1)-N(2)	171.2(1)	170.3
C(17)-Re(1)-N(2)	96.0(1)	89.4
C(18)-Re(1)-N(2)	101.3(1)	102.9
N(1)-Re(1)-N(2)	74.7(1)	74.3
C(16)-Re(1)-Br(1)	92.7(1)	90.4
C(17)-Re(1)-Br(1)	177.6(1)	176.1
C(18)-Re(1)-Br(1)	91.6(1)	94.1
N(1)-Re(1)-Br(1)	85.74(7)	82.6
N(2)-Re(1)-Br(1)	82.07(7)	88.8
O(1)-C(16)-Re(1)	178.6(3)	178.3
O(2)-C(17)-Re(1)	179.5(3)	179.4
O(3)-C(18)-Re(1)	179.9(3)	176.8
Torsion	Degrees (°)	
	Experimental	Calculated
N(1)-C(6)-C(1)-N(2)	-15.4(4)	-15
N(2)-C(5)-C(11)-N(3)	141.1(3)	136

Table 2.5 Selected Distances, Angles, and Torsions for **2.5**.

Axial CN			Planar CN		
Bond	Distance (Å)		Bond	Distance (Å)	
	Exp.	Calc.		Exp.	Calc.
Re(2)-C(35)	2.148(7)	2.14	Re(1)-C(19)	2.105(8)	1.99
Re(2)-C(36)	1.926(6)	1.94	Re(1)-C(16)	1.928(5)	2.09
Re(2)-C(37)	1.954(7)	1.97	Re(1)-C(18)	1.96(1)	2.01
Re(2)-C(38)	1.902(9)	1.92	Re(1)-C(17)	1.918(7)	1.90
Re(2)-N(5)	2.242(7)	2.29	Re(1)-N(1)	2.253(5)	2.32
Re(2)-N(6)	2.168(5)	2.20	Re(1)-N(2)	2.176(4)	2.19
C(35)-N(8)	1.138(9)	1.16	C(19)-O(3)	1.17(1)	1.15
C(36)-O(4)	1.145(8)	1.15	C(16)-N(4)	1.149(7)	1.16
C(37)-O(5)	1.151(9)	1.15	C(18)-O(2)	1.14(1)	1.14
C(38)-O(6)	1.17(1)	1.15	C(17)-O(1)	1.130(8)	1.16
Angle	Degrees (°)		Angle	Degrees (°)	
	Exp.	Calc.		Exp.	Calc.
C(36)-Re(2)-C(38)	87.7(3)	87.2	C(16)-Re(1)-C(17)	87.8(3)	90.2
C(36)-Re(2)-C(37)	88.0(3)	89.9	C(16)-Re(1)-C(18)	87.0(3)	84.8
C(36)-Re(2)-C(35)	92.1(3)	93.4	C(16)-Re(1)-C(19)	92.5(3)	88.4
C(38)-Re(2)-C(37)	88.5(3)	91.0	C(17)-Re(1)-C(18)	88.7(3)	88.4
C(38)-Re(2)-C(35)	90.8(3)	91.6	C(17)-Re(1)-C(19)	90.5(3)	87.7
C(37)-Re(2)-C(35)	179.2(3)	175.9	C(18)-Re(1)-C(19)	179.1(3)	172.2
C(36)-Re(2)-N(5)	100.6(3)	102.6	C(16)-Re(1)-N(1)	102.2(2)	98.1
C(36)-Re(2)-N(6)	174.2(3)	175.7	C(16)-Re(1)-N(2)	175.9(2)	172.0
C(38)-Re(2)-N(5)	169.3(3)	170.1	C(17)-Re(1)-N(1)	168.3(3)	170.5
C(38)-Re(2)-N(6)	96.6(3)	96.2	C(17)-Re(1)-N(2)	95.9(3)	97.5
C(37)-Re(2)-N(5)	98.4(2)	89.4	C(18)-Re(1)-N(1)	97.7(3)	88.5
C(37)-Re(2)-N(6)	96.0(2)	92.6	C(18)-Re(1)-N(2)	94.8(3)	93.4
C(35)-Re(2)-N(5)	82.3(2)	87.5	C(19)-Re(1)-N(1)	83.2(2)	96.3
C(35)-Re(2)-N(6)	83.9(2)	84.0	C(19)-Re(1)-N(2)	85.7(2)	93.9
N(5)-Re(2)-N(6)	74.7(2)	74.0	N(1)-Re(1)-N(2)	73.9(2)	73.7
O(6)-C(38)-Re(2)	179.4(7)	178.0	O(1)-C(17)-Re(1)	178.2(7)	177.6
O(5)-C(37)-Re(2)	175.5(6)	179.4	O(2)-C(18)-Re(1)	172.0(7)	176.4
N(8)-C(35)-Re(2)	178.0(6)	176.4	O(3)-C(19)-Re(1)	178.0(6)	176.6
O(4)-C(36)-Re(2)	179.0(7)	177.3	N(4)-C(16)-Re(1)	178.7(6)	178.1
Torsion	Degrees (°)		Torsion	Degrees (°)	
	Exp.	Calc.		Exp.	Calc.
N(5)-C(20)-C(25)-N(6)	14.5(9)	14	N(1)-C(1)-C(6)-N(2)	12.5(8)	15
N(5)-C(24)-C(30)-N(7)	41(1)	136	N(1)-C(5)-C(11)-N(3)	43.7(9)	137

Table 2.6 Selected Distances, Angles, and Torsions for **2.2**.

Bond	Distance (Å)	
	Experimental	Calculated
Re(1)-C(16)	1.926(9)	1.92
Re(1)-C(17)	1.975(10)	1.91
Re(1)-N(1)	2.119(7)	2.13
Re(1)-N(2)	2.080(7)	2.09
Re(1)-N(3)	2.126(7)	2.13
Re(1)-Cl(1)	2.489(3)	2.53
N(1)-N(3)	4.14(1)	4.15
C(16)-O(1)	1.14(1)	1.16
C(17)-O(2)	1.05(1)	1.16
Angle	Degrees (°)	
	Experimental	Calculated
C(16)-Re(1)-C(17)	91.5(4)	89.2
C(16)-Re(1)-N(2)	173.7(4)	172.0
C(17)-Re(1)-N(2)	94.6(3)	98.8
C(16)-Re(1)-N(1)	103.9(3)	103.0
C(17)-Re(1)-N(1)	92.7(3)	93.4
N(2)-Re(1)-N(1)	77.3(3)	76.7
C(16)-Re(1)-N(3)	101.8(3)	103.0
C(17)-Re(1)-N(3)	91.7(3)	93.4
N(2)-Re(1)-N(3)	76.6(3)	76.7
N(1)-Re(1)-N(3)	153.7(3)	153.2
C(16)-Re(1)-Cl(1)	91.8(3)	89.1
C(17)-Re(1)-Cl(1)	176.5(2)	178.3
N(2)-Re(1)-Cl(1)	82.1(2)	82.9
N(1)-Re(1)-Cl(1)	85.4(2)	87.0
N(3)-Re(1)-Cl(1)	88.7(2)	87.0
O(1)-C(16)-Re(1)	177.9(9)	179.1
O(2)-C(17)-Re(1)	173.2(8)	179.2
Torsion	Degrees (°)	
	Experimental	Calculated
N(1)-C(5)-C(6)-N(2)	1(1)	2
N(2)-C(10)-C(11)-N(3)	-4(1)	-2

Table 2.7 Selected Distances, Angles and Torsions for Acetonitrile Adduct of **2.8**.

Bond	Distance (Å)	
	Experimental	Calculated
Re(1)-C(16)	1.889(4)	1.93
Re(1)-C(17)	1.885(3)	1.93
Re(1)-N(1)	2.091(3)	2.10
Re(1)-N(2)	2.135(3)	2.15
Re(1)-N(3)	2.131(3)	2.15
Re(1)-N(4)	2.160(3)	2.15
N(2)-N(3)	4.138(4)	4.18
C(16)-O(1)	1.170(4)	1.16
C(17)-O(2)	1.171(4)	1.15
Angle	Degrees (°)	
	Experimental	Calculated
C(16)-Re(1)-C(17)	87.69(16)	88.1
C(16)-Re(1)-N(1)	175.95(12)	176.1
C(17)-Re(1)-N(1)	96.35(12)	95.8
C(16)-Re(1)-N(3)	103.81(13)	103.6
C(17)-Re(1)-N(3)	94.03(12)	92.3
N(1)-Re(1)-N(3)	76.20(10)	76.3
C(16)-Re(1)-N(2)	103.58(13)	103.6
C(17)-Re(1)-N(2)	93.73(12)	92.3
N(1)-Re(1)-N(2)	75.99(10)	76.3
N(3)-Re(1)-N(2)	151.77(11)	152.5
C(16)-Re(1)-N(4)	90.50(14)	88.5
C(17)-Re(1)-N(4)	178.10(12)	176.6
N(1)-Re(1)-N(4)	85.46(10)	87.6
N(3)-Re(1)-N(4)	86.94(10)	88.5
N(2)-Re(1)-N(4)	86.15(10)	88.5
O(1)-C(16)-Re(1)	179.1(3)	178.8
O(2)-C(17)-Re(1)	178.0(3)	178.9
Torsion	Degrees (°)	
	Experimental	Calculated
N(1)-C(1)-C(6)-N(2)	1.7(4)	1
N(1)-C(5)-C(11)-N(3)	-1.8(4)	-1

Chapter 3

Photocatalysis of CO_2

3.1 Introduction

Only 6 years after the photophysical properties of Re^I complexes using 2,2'-bipyridine were characterized,[46] Hawecker, Lehn, and Ziessel showed the effectiveness of the compound for the photocatalytic reduction of CO_2.[66] Since then, many have shown the efficacy of a wide range of α-diimino complexes for the reaction[67,132,145] and expansion of the systems to bimetallic complexes with ruthenium and osmium as electron transfer agents has produced a wide range of results.[114,118,146] The mechanism of reduction has been subject of some debate: while mechanisms have been proposed since Lehn et. al. soon after their original publication,[67] modifications have been submitted routinely over the past decades.[87,118,119,147–151]

The development of a novel terdentate geometry and the associated increase in photon absorption at lower energies of the catalyst warranted investigation of the CO_2 reduction capabilities, having overcome the criticism of only absorbing high energy photons.[122] The terdentate complexes were tested and compared to the bidentate, and to the previously proven catalyst κ^2(bipy)Re$(CO)_3$Cl.

3.2 Photocatalytic Reactions with New Compounds

The photocatalytic cycle is, simply, a photon-induced MLCT, followed by the extraction of an electron from a sacrificial reductant. This negatively charged radical species sheds the halide anion, opening up a reaction site. Reduction of CO_2 yields any number of CO, H_2O, formate (HCO_2^-), or bicarbonate (CO_3H^-), depending on the mechanistic pathway (see Scheme 4.1). Further discussion and a proposal of a new mechanism geometry based on computational and experimental data can be read in chapter 4.

3.2.1 Conditions

Reaction conditions in use in literature have remained typically unchanged since the original papers. A mixture of DMF with either Triethanolamine (TEOA) or Triethylamine (TEA) at a 5:1 ratio is used to make a 1.0 mM solution of catalyst, with 'excess' (depending on reference, a 1.1 to 25 molar ratio) electrolyte salt (typically Et_4NX or t-Bu_4NX, where X = halide from catalyst) added as a stabilizer. Solutions are degassed by bubbling of CO_2 and a pure CO_2 headspace is left to form over the solution. The reaction of 4 mL of catalyst solution in a 30 mL sealed glass vial is monitored via Gas Chromatography (GC) analysis of the headspace, using a HP gas chromatograph with a 15 m CARBONPLOT column with 0.320 mm inner diameter and 1.50 μm film in a 40 °C oven. The instrument is fitted with a Thermal Conductivity Detector (TCD), and, while using He as a carrier gas, is able to resolve CO and CO_2 completely.

3.2.2 Experimental Results

Both bidentate and terdentate κ^n(terpy)Re$(CO)_{5-n}$X (n=2, 3) **2.1** and **2.2** complexes show no activity for CO_2 reduction. Modification of testing time, light source, product

Chapter 4

Mechanism of CO_2 Reduction

4.1 Introduction

Within two years of the appearance of the originally reported bipyridine rhenium (I) catalyst, experimental studies on the mechanism of the photocatalytic reduction of CO_2 were available in the literature.[70,122] Studies continue on the mechanism up to the present day,[68,118,147,155–160] utilizing new investigative techniques as they become available to elucidate transition states and transient intermediates *in situ*.

The mechanistic studies performed analyze CO_2 reduction both photocatalytically and electrocatalytically on Re compounds. The electrocatalytic activity was demonstrated by Hawecker *et al.* only a year after the photochemistry first appeared.[161] Both methods involve similar cycles, and have been treated interchangeably by some authors.[147,150,151] The difference between electrocatalytic and photocatalytic methods is the production of the excimer species, not the reduction at the active site. Electrochemical methods have been employed with the hope of utilizing CO_2 and H_2O together for the direct formation of methane and oxygen, however this problem is highly complex and the target remains elusive.[104,105]

Investigation includes the use of DFT methods to elucidate geometries of intermediates and transition states for the multi-step cycle. Transition metal catalysis is a non-trivial problem computationally, particularly when considering a metal from the lower period. These elements contain a large amount of electrons, many of which can be involved in non-covalent interactions with the ligands and catalyzed products. Obtaining good approximate wave functions for these complex, large systems becomes non-trivial and computationally expensive. Likely for this reason, no broad review of the mechanisms of CO_2 reduction by Re^I catalysts, investigated by DFT methods, has ever been made available in the literature.

This section will provide the first complete DFT mechanistic study, from excimer formation, through key intermediates of CO_2 binding and reduction, to the release of products and reformation of the catalyst. Various mechanistic pathways will be investigated, and experimental observations will be considered with the computational results. A new mechanism geometry will be proposed, tackling previously unexplained properties of the reactions.

4.2 Mechanism Pathways

Prior work in the literature has proposed three general mechanistic pathways for the photoreduction of CO_2.[68,87,147,157] In general, as seen in Scheme 4.1, these pathways result in the formation of CO and H_2O, formate (HCO_2^-), or bicarbonate (HCO_3^-) anions. The formation of bicarbonate proceeds via the formation of a CO_2 bridged dimer that undergoes a CO_2 insertion reaction to ultimately produce bicarbonate and a molecule of CO. Production of formate requires the formation of a Re-H complex, which undergoes CO_2 insertion. The formation of CO without bicarbonate or formate by-products occurs via the coordination of CO_2 to an open site on the metal, followed by a double proton

of CO.

4.2.1 Excimer Formation and Decomposition of the Sacrificial Amine

All of the mechanistic pathways require the formation of a common excimer species, the radical $17e^-$ complex (Scheme 4.2). This occurs through the absorption of an incident photon with enough energy to promote an electron from the metal d-orbital to the ligand π^* orbitals of the ground state catalyst, **4.01**, forming the triplet Metal-Ligand Charge Transfer (3-MLCT) complex $^{\mathbf{3}}\mathbf{4.01}^{\mathbf{MLCT}}$. This excitation requires approximately 50 kcal/mol, sourced from absorbed light. The pseudo-oxidized, electron-deficient metal atom extracts an electron from the sacrificial amine present in the reaction solution to return to the Re^I state (**4.02**). However, this complex is formally a radical anion with the lone electron located in the ligand π system, thus a halide (**4.04**) is lost to return to the neutral radical excimer species in solution, **4.03**. This electron extraction to form the radical anion catalyst and the radical cation amine is highly endothermic in the gas phase, costing over 80 kcal/mol, but in DMF it is exothermic by 5 kcal/mol. The difference in energies demonstrates the importance of performing calculations in a simulated solution; steps that may have insurmountable energy barriers in the gas phase become possible once solvation is considered.

A modestly endothermic dissociation of the chloride (15.44 kcal/mol in DMF) allows for the formation of the triplet 17 e^- excimer species **4.03**, from which the pathways discussed in following subsections may diverge.

It is important to note that some studies suggest the solvent coordinates with the excimer species.[87,160] This solvent coordination is expected to stabilize the excimer species in solution prior to reaction with CO_2.[183] The coordination provides approximately

11 kcal/mol of stabilization (calculated via DFT). However, this event has no bearing on the overall reaction energies, as the coordination and subsequent loss of solvent is an energetically neutral occurrence and was not examined in detail.

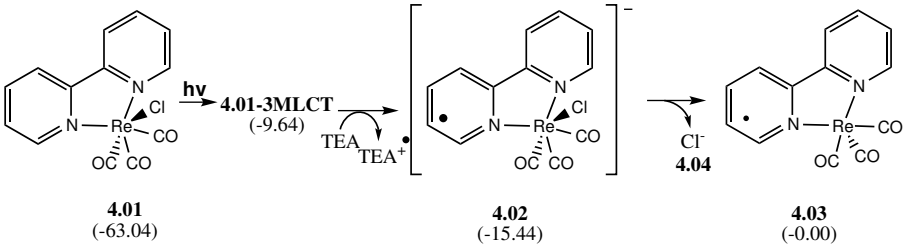

Scheme 4.2 Formation of the excimer species via absorption of a photon and oxidation of the sacrificial amine. Energy in kcal/mol relative to the excimer **4.03** is shown in brackets for each compound.

The decomposition route of the sacrificial amine was first identified by Kalyansundarem in 1978,[162] and is summarized in Scheme 4.3. Although this work showed the decomposition of TEOA, the mechanism for decomposition of TEA is analogous. This decomposition is critical due to the protons it provides to the reaction mixture, and the presence of a simple second electron abstraction from the decomposition product. Upon absorption of a photon by the catalyst, the amine **4.05** is converted to the radical cationic species ($Et_3N^{+\bullet}$, **4.06**). This undergoes a proton transfer to a second molecule of the sacrificial reductant. The transfer removes a proton from the carbon α to the central nitrogen, leaving it a neutral radical species (forming **4.07**). This is then able to react in the catalytic cycle to provide a second electron and form the ethene-diethylamino compound **4.26**. Triethylammonium is produced as well (**4.08**), which is a proton source for the formate and water-gas shift mechanistic pathways. This step is slightly exothermic, with energy releases of 1 kcal/mol in the gas phase, and nearly 3 kcal/mol in DMF.

Energies of each step of the reaction are listed in Table 4.1. The values show a significant 'uphill' series of steps requiring significant energy input. This energy is supplied

putational analysis consists of investigation from the formed CO_2 linked dimer, through the release of CO, terminating at the carbonate linked dimer. Studies typically build the dimer as a tri-molecular step, or start with a Re−Re bound catalyst dimer and the insertion of CO_2.[150] However, the formation of the $[L_2Re(CO)_3]_2$ is exceptionally slow in the presence of solvent, with a rate constant 8 orders of magnitude below the formation of the solvent-stabilized radical $^{\bullet}L_2Re(CO)_3$(solv) complex,[183] and the $[L_2Re(CO)_3]_2$ dimer is considered completely unreactive to CO_2.[147]

Table 4.2 shows the potential energy change in each step of the reaction. The potential energy diagram is shown in Figure 4.3. The computed intermediate and transition state structures are shown in Figure 4.2.

Table 4.2 Energies for the reaction steps in the 'carbonate' pathway

Steps	Energy(gas)[a]	Energy(dmf)[b]
4.03 + **4.09** → **4.11**	-0.25	6.37
4.11 + **4.03** → **4.12**	-31.56	-42.39
4.12 + **4.09** → **TS4.13**	-21.37	-22.81
TS4.13 → **4.14**	34.01	30.62
4.14 → **TS4.15**	21.10	22.46
TS4.15 → **4.16** + **4.10**	-24.36	-24.84
4.16 → **4.17** + **TS4.19**	317.95	262.71
4.17 + **TS4.19** + **4.04**(×2) → **4.01**(×2) + **4.18**	-180.55	-239.63

[a] TPSS energy in kcal/mol.
[b] TPSS energy in kcal/mol with COSMO solvation in DMF.

The mechanism begins with the addition of a CO_2 molecule to the excimer **4.03**, forming **4.11**. This is a very weakly bound species when solved in a simulated DMF environment; in the gas phase this transition complex will not solve. Energies for the gas phase for this compound are calculated as single point energies from the solvated structure. The DMF solved structure has a Re-C bond length of 2.51 Å, and O-C-O bonding angle of 142°, when compared to the Re−C distances of rhenium carbonyls

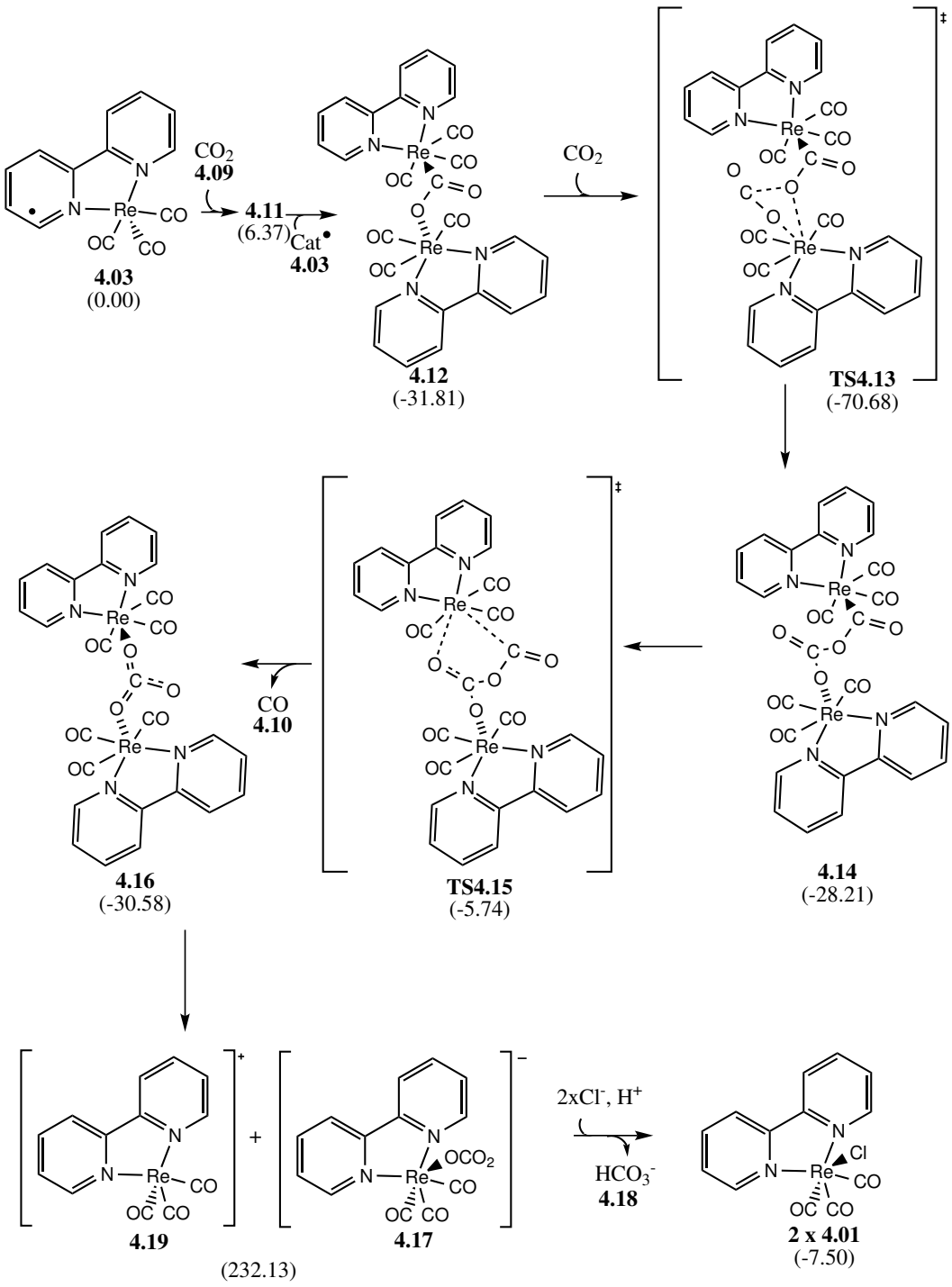

Scheme 4.4 The 'bicarbonate' mechanistic pathway. Energy in kcal/mol relative to the excimer **4.03** is shown in brackets for each compound.

contains C−O single bonds of length 1.28 Å, and C=O double bonds of 1.44 Å, longer than expected by about 0.1 Å for both sp^2 carbon-oxygen single or double bonds.[190] Bond angles are typically just under the idealized 120° expected as well. Due to the linker, the two catalyst ligand bipyridines have moved from a nearly co-planar geometry to a nearly perpendicular geometry. Re-C and Re-O bonds remain constant in length compared to **4.12**. The formation of a 5 membered ring transition state structure **4.15** costs 22 kcal/mol. This leads to the release of the CO and the formation of a carbonate linked dimer, **4.16**, resulting in a net energy decrease of -2.4 kcal/mol, and returning the catalyst ligands to a more co-planar orientation. The carbonate dimer species is left to decompose to a catalyst cation **4.19** with an open site, and the carbonate adduct **4.17**. This carbonate dianion may pick up a proton before or after the disassociation to the catalyst cationic species, resulting in the released of the bicarbonate species to solution (**4.18)** when the catalyst is returned to ground state **4.01** with addition of a chloride. The decomposition of the bicarbonate dimer species is very endothermic, by 262 kcal/mol in DMF. This is due to the charge separations that occur, while COSMO solvation stabilizes these charged species, it does not accurately simulate a system with an ionic strength similar to what could be expected in the experimental reaction. The Gibbs energy for this step was calculated to be -11.4 kcal/mol in solution, with an additional -17 kcal/mol for the anion exchange, signifying the thermodynamic favourableness of this transformation. The presence of excess molar equivalents of an electrolyte such as tetraethylammoniumchloride ensures a surplus of chloride anions are in solution and are an additional force for conversion, according to Le Châtelier's principle.

4.2.3 The 'Formate' Pathway

In comparison to the catalytic dimer formed in the bicarbonate pathway above, the formate formation occurs via a much simpler mechanism. This mechanism is shown in the green box in Scheme 4.1, with details shown in Scheme 4.5. The addition of a hydrogen to the open site axial to the metal occurs via the simultaneous electron and proton transfer from a by-product of the reduction of the amine. CO_2 inserts into this metal hydride bond, resulting in the formate ligand bonded through the oxygen center.[191–193] Separation of the weak metal-oxygen bond allows for the substitution of the halide to the cationic metal centre.

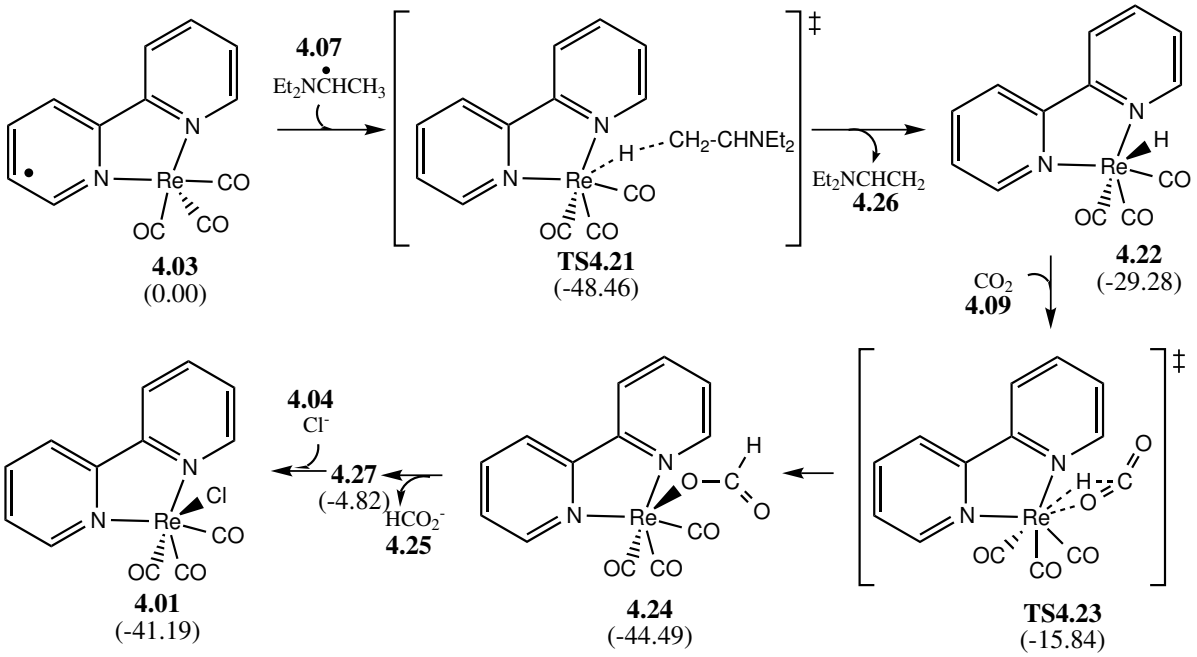

Scheme 4.5 The 'formate' mechanistic pathway. Energy in kcal/mol relative to the excimer **4.03** is shown in brackets for each compound.

Table 4.3 shows the potential energy change in each step of the reaction. The computed intermediate and transition state structures are shown in Figure 4.4.

After formation of the excimer **4.03**, the radical species extracts a hydrogen atom

in this variation. When a molecule of CO_2 approaches, the transition state of a pseudo-septacoordinate species **4.23** forms. The Re-H bond increases in length to 2.16 Å, the Re-O bond is 2.88 Å, and the O-Re-H angle is very tight, at only 45.3°. This step completes with 28.66 kcal/mol energy release to form the formato anion complex **4.24**.

The formato anion **4.24** contains a Re-O bond of 2.15 Å, consistent with previously discussed rhenium - oxygen bonds. This formate dissociates with a chloride addition, the exchange is endothermic by less than 3 kcal/mol overall, but the charge separated transition state formation is endothermic by nearly 40 kcal/mol in DMF (or 140 kcal/mol in gas phase). As discussed with the bicarbonate mechanism, this large cost is due to the charge separation that occurs. The calculated Gibbs energy for the formation of the charge separated transition state is -12.7 kcal/mol in solvent, showing the thermodynamic favourableness of this exchange. Further reactions of the formato anion in solution are not investigated, but the anion may remain deprotonated in the slightly basic environment.[129]

It is possible that the mechanistic cycle restarts with **4.24** absorbing a photon instead of substituting for the chloride. This would not affect the next catalytic cycle; either anion is lost in formation of the excimer.

Some attempts were made at performing the CO_2 binding reaction by alternative geometries. While direct σ bonding from a metal to an oxygen atom in the CO_2 molecule (as η^1-OCO) has been observed in a few systems (including photoreduction of CO_2 on other metal systems),[194–196] this geometry is rare.[197–199] Attempts to coordinate CO_2 in an η^1-OCO geometry failed to converge both in gas and solution phase, as CO_2 was ejected from the complex. Binding of CO_2 to the metal through π coordination of the C=O bond is more common,[198,199] but these structures failed to solve in the current DFT system as well.

4.2.4 The 'Water-Gas Shift' Pathway

The water-gas shift mechanism involves the addition of two protons from the reductant to a CO_2 molecule bound to the metal centre, as shown in the blue box in Scheme 4.1. The mechanism is shown in greater detail in Scheme 4.6. The first proton addition yields an acid species, this is dehydrated via the second addition of a proton and the release of one molecule of H_2O. The resulting tetracarbonyl cationic species is able then to release an axial carbonyl to return to the ground state. While any of the carbonyl groups could be labile, either of the carbonyl ligands at the axial positions are the ones actively replaced by the halide to return to the starting catalyst.[180]

Table 4.4 shows the potential energy change in each step of the reaction. The potential energy surface is shown in Figure 4.7. The computed intermediate and transition state structures are shown in Figure 4.6.

Table 4.4 Energies for the reaction steps in the 'water-gas shift' mechanism

Steps	Energy(gas)[a]	Energy(dmf)[b]
4.03 + **4.09** → **4.31**	-0.25	6.37
4.31 + **4.07** → **TS4.32**	-34.68	-46.72
TS4.32 → **4.33** + **4.26**	15.33	11.64
4.33 → **4.38** + **4.39**	-6.51	8.88
4.38 → **4.27** + **4.10**	40.89	35.57
4.27 + **4.04** → **4.01**	-141.77	-36.37

[a] TPSS energy in kcal/mol.
[b] TPSS energy in kcal/mol with COSMO solvation in DMF.

This mechanistic pathway appears to begin by the same addition of CO_2 that is seen in the bicarbonate mechanism (see subsection 4.2.2), forming **4.11**. As before, the complex is only weakly coordinated, and requires solvation effects to solve computationally. The added CO_2 is able to extract a hydrogen from the previously-reduced sacrificial amine **4.07** with a net energy change of -35.1 kcal/mol in DMF, again allowing the formation of

Chapter 5

TurboControl

The analysis of the mechanism using computational methods required a significant amount of manual set-up and analysis work of computational input and output files. The calculations required hundreds different molecules, intermediates, or transition state candidates to be calculated in multiple different environments, with the final mechanism employing 38 species in gas and solvated systems. These calculations typically require intervention or set-up of intermediate steps to be able to fully elucidate all of the required information, for example, the set-up of frequency calculations after a geometry optimization to ensure ground state or transition state geometries.

Additionally, while TurboMole contains much faster optimization code for DFT calculations, the user interface is exceptionally user-unfriendly and involves an abrasive interactive text prompt environment. This contrasts to Gaussian 09, which is significantly more popular, particularly due to the user-friendliness of the GaussView graphical user interface (GUI), despite concerns about the speed of optimization of large or complex molecules.

These two factors prompted the development of a new program, TurboControl, written in Python, with the goal of combining the user friendliness of GaussView on top of the

optimization efficiency of TurboMole. This program allows a user to prepare the input files in GaussView, modify them slightly in any text editor available to them, then run a batch calculation on the files. TurboControl monitors the computational jobs, resubmitting for frequency calculations when optimization is complete if requested, and using the TurboMole tools available when required to ensure ground state or first transition state geometries are discovered. TurboControl then creates a single output file, providing the energy and first frequency vibration of each molecule. Additional commands can instruct TurboControl to run in a solution, do single-point energy calculations, or gather more in-depth thermodynamic information from the outputs using TurboMole's tools.

TurboControl provides this hands-off management of jobs allowing the user to spend more time in data analysis, experimental work, or to be able to produce data at a significantly higher rate compared to the manual setup and monitoring of jobs. TurboControl also contains a single job initiation script entitled TurboGo to allow for the use of the input files without the overhead of the job managing.

This section will describe the development, features and usage of the TurboControl code in more detail.

5.1 Development

TurboControl began as a script for the simple setup and submission of jobs in TurboMole from Gaussian input files. The jobs were submitted to the 'wooki' computing cluster managed by the Woo lab, available at the University of Ottawa. This computing cluster consists of approximately 1000 CPU cores, running the CentOS distribution of Linux available in the Rocks software distribution. The GridEngine queuing system ensures fair usage of computing cores for each user, and maximizes throughput by managing computational jobs.

TurboControl initially submitted jobs and monitored their successful completion or failure. Development quickly expanded to include automatic resubmission for frequency analysis of geometry optimization jobs, required to determine the success of finding an energy minima (stationary point) instead of a transition state. TurboMole contains multiple ways of determining the ground state frequency of a geometry optimized molecule, TurboControl is granular enough to utilize whichever method is requested, or will default to a particular method if none is requested explicitly. While some methods are parallel calculations in TurboMole, others are able to utilize only a single processor core. Resubmitting jobs to the cluster's queue after each step ensures computational resources are not wasted, they are able to be shared appropriately by the queue.

As the complexity of the mechanistic study (see chapter 4) increased to include analysis of thermodynamic data, calculation of transition states, calculation in solution phases, and more, the capabilities of TurboControl were developed to meet these increased demands.

TurboControl is now able to handle large batches of input, with jobs of varying complexity and monitor them through successful completion or failure of the TurboMole calculation. Analysis of the computational jobs is performed to simply highlight DFT energies, first computed normal mode frequencies, and thermodynamic properties (if requested).

Development of TurboControl contained extensive testing at every step. Each function was tested as extensively as possible, including edge cases, error cases, and null inputs. This testing minimizes runtime errors, reducing the frequency of crashes of the code. Some code was unable to be subjected to programmed testing, the code interacting with the TurboMole scripts directly has been tested manually by developing test use cases. Test coverage can be seen in Appendix E, Code Details.

Code was written to be 'object oriented', that is, the code treats every molecule and job as an object, with defined properties, functions, and methods to manipulate these objects. This is a well defined coding style utilized when dealing with many items of similar type that contain data, when that object can be manipulated, activated, or modified. The data in the object is not modified directly, changes to the data is accessed via 'methods' that are properties of the object.

The code was written to be compliant with popular best practices, especially those designed for the Python language and described in 'PEP8'.[200] Deviations from the style guide were minimized and permitted only in special cases. Proper in code documentation was included as well, using both docstrings and inline comments.[201] This ensures code readability and simplifies future development by any author. The entire project is approximately 5500 lines of code, including tests, helper scripts, licence, and readme files.

5.2 Usage

TurboControl is available freely on the internet, and is a fully open-source project.[202] The code may be downloaded by anyone and be installed and used without prior permission for personal, academic, or commercial purposes, provided that the original software license remains with the code. TurboControl works only with the stated versions of software in the 'readme' file available with the code on the internet (and included in Appendix E). The software requires no installation prior to use, and has very few dependencies beyond the typically installed packages on a Unix or Linux system.

TurboControl and TurboGo are not quantum mechanical packages themselves, they require a properly licensed installation of TurboMole to perform calculations. Additionally, while GaussView may be used to prepare the input files, modification of the files by

hand in a text editor is required to access most features, GaussView is not required for the use of TurboControl.

5.3 Conclusions

TurboControl and TurboGo are two scripts developed to maximize throughput and minimize operator involvement in large computational studies utilizing TurboMole. Development of these scripts is not limited to the scope of the thesis, an open source licence and source code freely available on the internet mean this project may be adopted and further developed by others who are interested in its use. The scripts are not quantum chemical packages themselves, a fully licensed copy of the TurboMole software is required for their usage.

Chapter 6

Conclusions

The target Re^{I} terdentate terpyridine compounds were successfully synthesized and fully characterized. The experiments resulted in the first crystalographically verified *mer*-κ^3-(N, N', N")-$Re(CO)_2X$ complexes. These terpyridine complexes are accessed via a simple, highly efficient, solid-state thermolysis pathway. These complexes expand the previously known α-diimino photophysical properties, with enhanced metal to ligand d-π^* electronic transitions than the associated bidentate compounds. These experimental observations are supported by computational TD-DFT results, providing a deeper understanding of frontier molecular orbital environments for these complexes.

The synthesized catalysts were tested for the photoreduction of CO_2. The α-triimino catalysts show no activity for the reduction of CO_2, in contrast to the known excellent bipyridine compounds, potentially due to the lack of fluorescence of the terdentate complexes, and the chelating ability of the pendant arm in the bidentate 2,2':6,2"-terpyridine ligand. These catalysts may be suitable for electrocatalytic reduction of CO_2, further investigation will be required.

Reaction mechanisms of the photocatalytic reduction of CO_2 by bipyridine catalysts were studied successfully with DFT methods. This study was the first to show the en-

tire catalytic cycle, from eximer formation to CO_2 insertion and to catalyst reformation. This study also resulted in the proposed new geometry for the production of CO with no carbonate or formate anions. This new geometry does not conflict with known experimental studies, yet avoids three-body mechanistic steps previously seen in literature. This geometry provides explanation for previously unexplained phenomenon of ^{13}CO ligand exchange in few turnovers.

Development of a tool for the rapid submission and automated job monitoring for the TurboMole program facilitated the mechanism investigation by maximizing computational throughput while minimizing set-up and analysis time for the user. The scripts increase the 'black box' nature of TurboMole, increasing the usability to include those unfamiliar with the program, and take advantage of the high performance of TurboMole relative to other computational suites. An open source licence and freely available source code mean this project may continue with other developers in the future

Appendix A

Experimental Procedures

Experimental synthesis and characterization data for the compounds discussed in this thesis are shown below by compound number:

A.1 General Methods

Synthesis reactions were set-up in a glovebox under a nitrogen atmosphere and performed under an inert atmosphere. Solvents were sparged with nitrogen and then dried by passage through a column of activated alumina using an apparatus purchased from Anhydrous Engineering. Deuterated chloroform and deuterated acetonitrile was dried using activated molecular sieves. Rhenium starting materials were purchased from Strem Chemicals and used as received. All other chemicals were purchased from Aldrich and used without further purification. NMR spectra were run on Bruker Avance 400MHz spectrometers with CD_3CN or $CDCl_3$ as solvent and internal standard. Elemental analyses were performed by Midwest Microlab LLC, Indianapolis IN. Solid state reactions were carried out in a Lindberg Blue M Mini-Mite Tube Furnace (model TF55035A-1). Infrared spectra were collected using an Agilent Technologies Cary FT-IR spectrome-

ter using a diamond ATR attachment. UV-Vis spectra were collected using a Agilent Technologies Cary 5000 UV-Vis spectrometer. TGA was performed on a TA Q5000 IR instrument: approximately 10-15 mg of each sample was placed in a ceramic sample pan which was heated at a rate of 5 °C/min up to 150 °C, followed by a rate of 2 °CC/min to 300 °C while being purged with N_2 at a flow rate of 25 mL/min. GC was performed using a HP gas chromatograph with a 15 m CARBONPLOT column with 0.320 mm inner diameter and 1.50 μ film in a 40 °C oven. The instrument is fitted with a TCD at 220 °C.

A.2 Computational Methods

For the UV-Vis and experimental correlation study, the structures of all species were optimized using Gaussian 09[135] employing the B3LYP[133,134] exchange-correlation (XC) functional. The LanL2DZ basis set/effective core potential[136] was used on Re and, the all-electron TZVP basis set[137] for the remaining lighter atoms. Frequency analysis of all structures was used to confirm the nature of the stationary points. Solvent effects were computed using the integral equation formalism variant of the PCM solvation model within Gaussian 09 for both the ground state and excited state TD-DFT calculations with DMSO as the solvent.[140,141] The UV-Vis absorption spectra were extracted using the Chemissian software.[203] In these calculations, a pseudo-Voigt band shape was employed with a default average band width at half-height of 2000cm^{-1}.

For the mechanism study, the ground and transition state structures and energies of all species were obtained by using TurboMole 6.5 software[163,164] with the TPSS meta-GGA XC functional.[165] The def2-TZVP basis set was used for all atoms.[137,166] The TurboMole program contains a number of optimizations to the original DFT algorithms,[167–175] decreasing the calculation time without compromising accuracy. Grimme's dispersion cor-

rection (version 3) was included in the calculations.[176] Intermediates and transition states were verified by frequency analysis.[172,177,178] The effects of solvation was calculated using the Conductor-like Screening Model (COSMO) implemented in TurboMole,[179] which is a continuum solvation model implicitly surrounding the solute molecule.

A.3 X-ray Crystallography

Crystals were mounted on thin glass fibers using paraffin oil. Prior to data collection crystals were cooled to 200.15K. Data were collected on a Bruker AXS SMART single crystal diffractometer equipped with a sealed Mo tube source (wavelength 0.71073 Å) APEX II CCD detector. Raw data collection and processing were performed with APEX II software package from BRUKER AXS53.[204] Diffraction data for sample **3** was collected with a sequence of 0.5° ω scans at 0, 120, and 240° in ϕ. Due to lower unit cell symmetry in order to ensure adequate data redundancy, diffraction data for **1**, **2** and **8** were collected with a sequence of 0.5° ω scans at 0, 90, 180 and 270° in ϕ. Initial unit cell parameters were determined from 60 data frames with 0.3° ω scan each collected at the different sections of the Ewald sphere. Semi-empirical absorption corrections based on equivalent reflections were applied.[205] Systematic absences in the diffraction data-set and unit-cell parameters were consistent with triclinic $P\bar{1}$ ($\mathcal{N}^{\mathcal{O}}2$) for compounds **1**, **2** and **8**, monoclinic **C**2/c ($\mathcal{N}^{\mathcal{O}}15$) for compound **3**. Solutions in the centrosymmetric space groups for all compounds yielded chemically reasonable and computationally stable results of refinement. The structures were solved by direct methods, completed with difference Fourier synthesis, and refined with full-matrix least-squares procedures based on F^2.

Solutions for **1** and **2** revealed that both these structures contain two compound molecules per asymmetric unit.

Initial refinement results for the compound **1** suggested presence of two non-merohedrally twinned domains. Two independent orientation matrices were found using CELL_NOW software.[206] Data set was re-integrated with two independent orientation matrices and consecutive model refinement was performed using HKLF5 format reflection data file. Twinning domain ratio coefficient (BASF) was successfully refined to 0.3794.

On the final model refinement stage for compound **2** thermal motion parameters for coordinated CO (-C(33)=O(3)) and Cl (Cl(2)) moieties as well as presence of unusually strong residual electron density peaks in one of the compound molecules suggested a positional CO / Cl disorder not related by symmetry. Disorder was successfully modeled with refined occupation ratio at one position CO / Cl = 70%:30%. Disorder of the second position was inversed in such way that overall occupancy summed up to one full CO and one full Cl ligands in the first coordination sphere of Re metal center. Set of geometrical (SADI) and thermal motion (SIMU, DELU) restrains were applied to achieve acceptable molecular fragment geometries and thermal motion parameter values.

For all the compounds hydrogen atoms positions were initially assigned from the residual electron density peaks coordinates. However, after initial placement all hydrogen atoms were treated as idealized contributions during the refinement. All scattering factors are contained in several versions of the SHELXTL program library, with the latest version used being v.6.12.[207]

X-Ray crystal structures are shown in Appendix B

A.4 (terpy-κ^2-N,N′)$Re(CO)_3Cl$ (2.1)

$Re(CO)_5Cl$ (201 mg, 0.556 mmol) and 2,2:6,2 terpyridine (129 mg, 0.553 mmol) were mixed in 60 mL of toluene. The reaction mixture was heated to 100C for 1 hour under N2. During this time the solution turned a bright red. Upon cooling a yellow precipitate

was formed. The solution was filtered, and the solid was washed with diethyl ether, and dried under vacuum. Compound **1** is a bright yellow powder that was isolated in 70 % yield (208 mg). Crystals were obtained from chloroform with addition of a small amount of hexanes as counter solvent. TGA: 8 % mass loss from 240-280 °C. FTIR: 2019, 1981, 1889 cm^{-1} (υ C=O). ^{1}H NMR (CD_3CN, 400 MHz): δ 9.06 (ddd, J=5.6, 1.7, 0.8 Hz, 1H), 8.77 (ddd, J=4.9 Hz, 1H), 8.49 (td, J=8.2, 1.5 Hz, 2H), 8.28 (t, J=7.9 Hz, 1H), 8.22 (td, J=8.1, 1.6 Hz, 1H), 7.96 (td, J=7.8, 1.8 Hz, 1H), 7.79 (dt, J=7.8, 1.1 Hz, 1H), 7.80 (dd, J=7.7, 1.0 Hz, 1H), 7.63 (ddd, J=7.6, 5.5, 1.2 Hz, 1H), 7.55 (ddd, J=7.6, 5.0, 1.0 Hz, 1H). Elemental analysis calculated (%) for [$C_{18}H_{11}ReClN_3O_3$]: C 40.11, H 2.06, N 7.80, found C 39.96, H 2.09, N 7.69.

A.5 (terpy-κ^3-N,N′,N″)Re(CO)$_2$Cl (2.2)

Compound **2.1** (101 mg, 0.187 mmol) was placed in a tube furnace and heated to 240 °C under N_2 flow for 60 minutes. A black solid was collected (90 mg) at 94 % yield based on the formula for **2**. Crystals were obtained from chloroform with addition of a small amount of hexanes as counter solvent. FTIR: 1872, 1788 cm^{-1} (υ C=O). ^{1}H NMR (CD_3CN, 400 MHz): δ 8.70 (ddd, J=4.7, 1.8, 0.9 Hz, 2H), 8.65 (dt, J=8.0, 1.0, 1.0, 2H), 8.47 (d, J=7.8 Hz, 2H), 8.03 (t, J=7.8 Hz, 1H), 7.95 (td, J=7.7, 7.7, 1.9 Hz, 2H), 7.43 (ddd, J=7.5, 4.8, 1.2 Hz, 2H). Elemental analysis calculated (%) for [$C_{17}H_{11}ReClN_3O_2$]: C 39.96, H 2.17, N 8.22, found C 39.62, H 2.09, N 7.99.

A.6 (terpy-κ^2-N,N′)Re(CO)$_3$Br (2.3)

$Re(CO)_5Br$ (191 mg, 470 mmol) and 2,2:62 terpyridine (129 mg, 0.553 mmol) were allowed to react under conditions analogous to the preparation of **1**. A bright yellow

powder was obtained, 0.223 g (0.382 mmol, 81 %). FTIR: 2012, 1910, 1886 cm^{-1} (υ C=O). ^1H NMR (CD_3CN, 400 MHz): δ 9.07 (ddd, J=5.6, 1.6, 0.9 Hz, 1H), 8.77 (ddd, J=4.6, 1.5, 0.8 Hz, 1H), 8.52 8.48 (m, 2H), 8.28 (t, J=7.9 Hz, 1H), 8.21 (td, J=8.0, 1.6 Hz, 1H), 7.97 (td, J=7.8, 1.8 Hz, 1H), 7.80 7.75(m, 2H), 7.63 (ddd, J=7.6, 5.5, 1.2 Hz, 1H), 7.55 (ddd, J=7.7, 4.9, 1.1 Hz, 1H). Elemental analysis calculated (%) for $[C_{18}H_{11}ReBrN_3O_3]$: C 37.06, H 1.90, N 7.20, found C 36.94, H 1.92, N 7.00.

A.7 (terpy-κ^3-N,N′,N″)$Re(CO)_2Br$ (2.4)

Compound **2.3** (182 mg, 0.312 mmol) was placed in an tube furnace and heated to 230 °C under N_2 flow for 60 minutes. A black solid was collected, 0.155 mg (0.279 mmol, 89 % yield). Crystals were obtained from chloroform with addition of a small amount of hexanes as counter solvent. FTIR: 1873, 1794 cm^{-1} (υ C=O). ^1H NMR (CD_3CN, 400 MHz): δ 8.95 (d, J=5.4 Hz, 2H), 8.24 (t, J = 8.1Hz, 4H), 8.05 (dd, J=8.2, 7.7 Hz, 1H), 7.90(td, J=7.9, 1.7 Hz, 2H), 7.63 (ddd, J=7.3, 5.5, 1.2 Hz, 2H). Elemental analysis calculated (%) for $[C_{17}H_{11}ReBrN_3O_2]$: C 36.76, H 2.00, N 7.57, found C 36.66, H 2.00, N 7.50.

A.8 (terpy-κ^2-N,N′)$Re(CO)_3CN$ (2.5)

To **2.3** (60 mg, 0.103 mmol), $AgCF_3SO_3$ (40 mg, 0.299 mmol) was added in 10 mL CH_2Cl_2. The reaction was stirred 18 h and kept dark under N_2 atmosphere. Solution was filtered to remove salts, then reduced in volume. Cold diethyl ether was used to precipitate product. Yellow-grey powder (**7a**) was collected by filtration, yielding 48mg (88 %). Crystals were grown from saturated chloroform with hexanes as countersolvent for X-ray crystallography. FTIR: 2013, 1905, 1884 cm^{-1} (υ C=O). ^1H NMR (CD_3CN,

400 MHz): δ 9.08 (dd, J=5.40, 0.49 Hz, 1 H), 8.78 (dd, J=5.10, 0.59 Hz, 1 H), 8.53 (dd, J=8.18, 0.93 Hz, 1 H), 8.50 (d, J=8.23 Hz, 1 H), 8.30 (t, J=7.90 Hz, 1 H), 8.23 (td, J=7.94, 1.57 Hz, 2 H), 7.98 (td, J=7.76, 1.71 Hz, 1 H), 7.80 (dd, J=7.79, 1.03 Hz, 1 H), 7.77 (d, J=7.74 Hz, 0 H), 7.64 (ddd, J=7.50, 5.50, 1.08 Hz, 1 H), 7.55 (ddd, J=7.62, 4.92, 0.98 Hz, 2 H). Elemental analysis calculated (%) for $[C_{19}H_{11}N_4O_3Re]$: C 43.10, H 2.09, N 10.58, found C 40.06, H 2.06, N 9.85.

A.9 (terpy-κ^3-N,N′,N″)Re(CO)$_2$CN (2.6)

Compound **2.5** (108 mg, 0.204 mmol) was placed in an tube furnace and heated to 220 °C under N_2 flow for 60 minutes. A black solid was collected, 88 mg (0.175 mmol, 86 % yield). ^{1}H NMR (CD_3CN, 400 MHz): δ 8.60(ddt, J=4.8, 1.7, 0.8, 0.8 Hz, 2H), 8.48 (dq, J=8.0, 1.0 Hz, 2H), 8.37 (dd, J=7.9, 0.8 Hz, 2H), 8.07 (dd, J=8.0, 7.6 Hz, 1 H), 7.94 (ddd, J=7.9, 7.5, 1.8 Hz, 2H) 7.43 (ddd J=7.4, 4.8, 1.2 Hz, 2H). Elemental analysis calculated (%) for $[C_{18}H_{11}N_4O_2Re]$: C 43.11, H 2.21, N 11.17, found C 40.26, H 2.67, N 9.60.

A.10 (terpy-κ^2-N,N′)Re(CO)$_3$OTf (2.7)

To **2.1** (80 mg, 0.148 mmol), $AgCF_3SO_3$ (46 mg, 0.179 mmol) was added in 10 mL CH_3CN. The reaction was stirred 18 h and kept dark. Solution was filtered to remove salts, then reduced in volume. Cold diethyl ether was used to precipitate product. Yellow-grey powder (**7a**) was collected by filtration, yielding 38 mg (40 %). Crystals were grown from saturated chloroform with hexanes as countersolvent for X-ray crystallography. FTIR: 2030, 1895, 1890 cm^{-1} (υ C=O), 1280, 1228, 1204 cm^{-1} (υ SO_3). ^{1}H NMR (CD_3CN, 400 MHz): δ 9.05 (ddd, J=5.5, 1.6, 0.8 Hz, 1H), 8.79 (ddd, J=4.9, 1.8, 1.1 Hz, 1H), 8.57

(dd, J=8.1, 0.9 Hz, 1H), 8.54 (dt, J=8.2, 1.1 Hz, 1H), 8.37 (t, J=7.9 Hz, 1H), 8.31 (td, J=8.0, 1.6 Hz, 1H), 8.03 (td, J=7.7, 1.7 Hz, 1H), 7.87 (dd, J=7.8, 1.0 Hz, 1H), 7.75 (dt, J=7.8, 1.1 Hz, 1H), 7.72 (ddd, J=7.4, 5.9, 1.1 Hz, 1H), 7.61 (ddt, J=7.7, 4.8, 0.5, 0.5 Hz, 1H). Elemental analysis calculated (%) for [$C_{19}H_{11}ReN_3O_6F_3S$]: C 34.97, H 1.70, N 6.44, found C 31.80, H 1.73, N 5.33.

Alternately, to **1** (72 mg, 0.134 mmol) was added 10 mL CF_3SO_3H (excess) and temperature was increased to 100 °C for 20 minutes. A black solution was neutralized with addition of 5% Na_2CO_3 in H_2O. Product was extracted with $CHCl_3$, then dried under vacuum to yield a brown solid (**7b**) (47 mg, 54 %).

A.11 (terpy-κ^3-N,N′,N″)Re(CO)$_2$OTf (2.8)

To **2.2** (77 mg, 0.143 mmol), $AgSO_3CF_3$ (47 mg, 0.183 mmol) was added in 15 mL CH_3CN. Solution was refluxed for 6 h in the dark under N_2 atmosphere. Solution was filtered, then reduced to minimal volume. Cold diethyl ether was added dropwise to precipitate product. Collected by filtration and washed with additional cold ether, yielding 75 mg (120 mmol, 80 %). Crystals grown from saturated methylene chloride, with hexanes as countersolvent for x-ray crystallography. FTIR: 1910, 1829 cm^{-1} (υ C=O), 1259, 1224, 1143 cm^{-1} (υ SO_3). ^{1}H NMR (CD_3CN, 400 MHz): δ 8.91(ddd, J=5.6, 1.6, 0.7 Hz, 2H), 8.32 (d, J=8.0 Hz, 2H), 8.28 (ddd, J=8.1, 1.4, 0.8 Hz, 2H), 8.19 (dd, J=8.8, 7.4 Hz, 1H), 8.02 (td, J=7.9, 1.5 Hz, 2H) 7.46 (ddd J=7.6, 5.6, 1.3 Hz, 2H). Elemental analysis calculated (%) for [$C_{18}H_{11}ReF_3SN_3O_5$]: C 34.62, H 1.78, N 6.37, found C 31.02, H 1.82, N 7.11.

Appendix E

TurboControl and TurboGo Manual

TurboControl is a series of scripts to run TurboMole jobs from Gaussian style inputs. The following is the user manual included with distributions of TurboControl

E.1 Introduction

Gaussian software is well known for the user friendly GUI it contains (via GaussView). TurboMole, another computational suite, is known for its speed and optimizations, but has a significantly higher learning curve and is less beginner friendly. This software is an attempt to be able to use the user friendly input from Gaussian to smooth over the use of TurboMole.

E.2 System Requirements

There are two user-facing scripts available, both written to work with TurboMole 6.1-6.5 on clusters using Grid Engine queuing software. The only tests of operation are on a system with the following details:

- Rocks 6.1 (Emerald Boa)/CentOS 6.3
- Open Grid Scheduler/Grid Engine 2011.11p1
- Python 2.7.3

Other systems, including different operating systems, different versions of Grid Engine or python, or on other systems, are not supported.

Python dependencies include:

- pexpect 3.2[208]
- openbabel (optional)[209,210]

Prior to running TurboGo or TurboControl, a valid installation of TurboMole must be available. On systems where computational modules must be loaded, TurboMole must have been loaded to the environment. Additionally, running the TurboMole environment configuration is recommended but not required prior to launching TurboGo or TurboControl:

```
$ source $TURBODIR/Config_turbo_env
```

E.3 Installation

Installation of TurboControl is very simple. Just extract the .tar.gz file available from the code repository at `https://github.com/pbulsink/turbocontrol/releases/latest`. Alternately, the source may be downloaded from `http://github.com/pbulsink/turbocontrol` and used without installation.

E.4 TurboGo

TurboGo is a script fun on an input file. It generates the inputs required for TurboMole jobs, and submits the job to the GridEngine queue before quitting. TurboGo is run with the following syntax:

```
$ turbogo [-h] [-v] [-q] file
```

positional arguments:

```
file                  Read input from gaussian-type input FILE.
```

More info on the input files is available below.

optional arguments:

- `-h, --help` Show this help message and exit
- `-v, --verbose` Run more verbose (show debugging info)
- `-q, --quiet` Run less verbose (show only warnings)

TurboGo saves a log file (turbogo.log) in the directory in which it is run. A second log file (define.log) will remain if the setup crashes or is terminated at some points, or if the script is run verbose.

TurboGo writes the final coordinates to final_geometry.xyz. If openbabel is installed, it will also write finalgeom.mol. The entire optimization is written to optimization.xyz for viewing with a molecular viewer, such as vmd.

E.5 TurboControl

TurboControl is a management script called from a parent directory containing sub directories of input files. Each input file must be in its own directory. The input file format

must be the same as the input format for TurboGo (listed above), with the extension '.in', '.inp', '.input', '.com', or '.gjf'. TurboControl reads the inputs and submits the jobs to the computational cluster queue. It then monitors running jobs to determine when the script has finished. If the job is an Opt-Freq, it prepares the frequency analysis and resubmits to the queue. TurboControl analyses completed Opt-Freq jobs for true optimization, and attempts to re-run jobs with modified geometries when Transition States are found. TurboControl will not get stuck on the same transition state, but will return a 'stuck' job. TurboControl is run with the following syntax:

```
$ turbocontrol [-h] [-v/-q] [-s]
```

Optional arguments:

- `-h, --help` Show this help message and exit
- `-v, --verbose` Run more verbose (show debugging info)
- `-q, --quiet` Run less verbose (show only warnings)
- `-s, --solvent` List available solvents for COSMO and quit

TurboControl outputs information every 3 hours on the status of the jobs. It writes a log file (`turbocontrol.log`) and may or may not leave other log files in each directory (depending on verbosity level). Ends when the last job finishes or crashes. Requires 1 node or can be run on the headnode (minimal resource consumption especially after initial job preparation and submission.)

TurboControl assists with analysis by outputting a `stats.txt` file as jobs complete. This file contains file details, optimization and frequency timing details, energy, and the first frequency. Additional information can be requested by including the `freeh` keyword (see below).

E.6 Input File Format

The input file format is similar to that well known by Gaussian users. A series of keywords, one per line and indicated by a '%', is followed by the 'route card' (specific job information). Charge and spin is indicated, then the molecule is shown in Cartesian format. This is followed by optional modifications to the TurboMole Control file. Note the location of blank lines in the example (Section 5.7).

E.6.1 Keywords

Keywords are as follows:

- `%nproc` - number of processors to use for the calculation job.
  - Synonym: `%nprocessors`
- `%arch` - parallelization architecture to use for the job.
  - Synonyms: `%architecture`, `%para_arch`
- `%maxcycles` - number of optimization iterations before failing.
- `%autocontrolmod` - DEFAULT - modify the `control` file to include optimizations to speed up the job.
- `%nocontrolmod` - do not modify `control` file as above.
- `%rt` - specify max expected runtime (for any part of job)in hours. Allows backfilling in GridEngine queue to speed up job submission. For example, for a 1 hour opt and 4 hour freq, submit at least a `rt` of 4

- `%cosmo` - use TurboMole's COSMO solvation model with the specified solvent or `None` to use the idealized solvent (epsilon = infinity). List of available solvents can be shown by running `turbocontrol -s`

Gaussian args, including `%nosave`, `%rwf=[file]`, `%chk=[file]`, and `%mem=[memory]` are silently ignored.

E.6.2 Route Card Options

Route cards take the form of the following:

`# [jobtype(s)] [joboption(s)]`

Job types available:

- `opt` - Perform a geometry optimization
- `freq` - Perform a frequency analysis. Specify method via numforce or aoforce. default = numforce
- `sp` - Perform a single point energy calculation.
  - Cannot be combined with Opt or Freq
- `ts` - Perform a transition state search to find 1 imaginary vibration.
  - Cannot be combined with Opt or Freq
- `prep` - Prepare the job but do not submit to queue.
  - Cannot be combined with Opt or Freq

Job options available:

- `ri` - Use TurboMole's ri approximation

- `marij` - Use TurboMole's marij approximation
  - Requires `ri`
- `disp` - Use TurboMole's implementation of Grimme's dispersion, version 3
- `aoforce` - Use aoforce for frequency jobs
- `numforce` - Use numforce for frequency jobs
- `freeh` - Use TurboMole's `freeh` thermodynamics data script to extract thermodynamic information after frequency analysis

E.6.3 Title

Following the Route cards, a blank line is added, then a line containing the title of the calculation. This can include any characters, spaces, etc., remaining on only one line. This is followed by a blank line.

E.6.4 Charge and Spin

Charge and spin are listed as two numbers separated by a space: charge spin (eg:0 1)

E.6.5 Geometry

Geometry in xyz coordinate format: Element xcoord ycoord zcoord. Z-matrix geometry is not supported by TurboControl or TurboGo.

E.6.6 Additional control File Modifications

Additional lines to be added or removed from control. Lines automatically added are, as required,:

```
$ricore 0
$paroptions ga_memperproc 900000000000000 900000000000
$parallel_parameters  maxtask=10000
$ricore_slave 1
$maxcor 2048
```

Additional lines may be added, or lines removed, by placing them after the geometry with a `$` (for addition) or `-$` (for removal).

E.6.7 Example Input File

An example input file for benzene in dmf:

```
%nproc=4
%arch=GA
%maxcycles=250
%rt=6
%cosmo=dmf
# opt freq b3-lyp/def2-TZVP ri marij numforce

Benzene Optimization & Frequency

0 1
C  0.000  1.396  0.000
C  1.209  0.698  0.000
C  1.209 -0.698  0.000
C  0.000 -1.396  0.000
C -1.209 -0.698  0.000
C -1.209  0.698  0.000
H  0.000  2.479  0.000
H  2.147  1.240  0.000
H  2.147 -1.240  0.000
H  0.000 -2.479  0.000
H -2.147 -1.240  0.000
H -2.147  1.240  0.000

$disp
-$paraoptions
```

E.7 Code Details

Coverage percentages of code unit tests are listed in Table E.1. Results are low for def_op, screwer_op, cosmo_op, freeh_op, turbocontrol, and turbogo because they contain many

lines of interacting with GridEngine or TurboMole. Testing is performed via monitoring the status of the scripts as they run in real conditions.

The code style is graded by PyLint and results are shown in Table E.2. PyLint describes coding style, adherence to guidelines, and readability. It does not describe code efficiency or usefulness.

Table E.1 Test Coverage of scripts in TurboControl.

Name	Statements	Missing	Excluded	Coverage
cosmo_op	106	70	1	34%
cosmo_op_test	17	1	0	94%
def_op	302	226	1	25%
def_op_test	20	1	0	95%
freeh_op	162	55	1	66%
freeh_op_test	27	1	0	96%
screwer_op	71	25	1	65%
screwer_op_test	11	1	0	91%
test_all	18	0	0	100%
turbocontrol	537	319	0	41%
turbocontrol_test	245	24	0	90%
turbogo	343	132	0	62%
turbogo_helpers	383	52	0	86%
turbogo_helpers_test	274	2	0	99%
turbogo_test	98	1	0	99%
TOTAL	2614	910	4	65%

Table E.2 PyLint Scores for Turbocontrol Code.

File	Score /10
test_all.py	2.22
turbogo.py	8.80
turbogo_test.py	6.97
turbocontrol.py	8.55
turbocontrol_test.py	7.18
turbogo_helpers.py	8.81
turbogo_helpers_test.py	7.45
def_op.py	8.18
def_op_test.py	5.71
screwer_op.py	7.36
screwer_op_test.py	6.67
freeh_op.py	8.71
freeh_op_test.py	6.79
cosmo_op.py	8.22
cosmo_op_test.py	6.67

E.8 Citing TurboControl

TurboControl, Turbogo, or any other parts of this code may be cited as:

Bulsink, Philip. TurboControl, v. 1.1.0. http://github.org/pbulsink/turbocontrol (accessed June 2014)

Change the version number to match the version that you used, and change the accessed date to when you installed or downloaded TurboControl.

E.9 License

Glossary of Terms

CCDC Cambridge Crystallography Data Centre

COSMO Conductor-like Screening Model

DFT Density Functional Theory

DMF N,N-dimethylformamide

DMSO Dimethylsulfoxide

FTIR Fourier Transform Infrared

GC Gas Chromatography

GUI graphical user interface

HOMO Highest Occupied Molecular Orbital

IRC Intrinsic Reaction Coordinate

LUMO Lowest Unoccupied Molecular Orbital

MLCT Metal-Ligand Charge Transfer

MO Molecular Orbital

NMR Nuclear Magnetic Resonance

PCM Polarizable Continuum Model

RWGSR Reverse Water-Gas Shift Reaction

TCD Thermal Conductivity Detector

TD-DFT Time Dependant Density Functional Theory

TEA Triethylamine

TEOA Triethanolamine

TGA Thermogravimetric Analysis

Bibliography

1. Zeise, W. C. *J. Physik und Chemie (Schweigger)* **1831**, *62*, 393–441.
2. Hunt, L. B. *Platinum Metals Review* **1984**, *28*, 76–83.
3. Griess, J. P.; Martius, C. A. *Compt Rendus.* **1861**, *53*, 922–925.
4. Birnbaum, K. *Ann. Chem. (Liebig)* **1868**, *145*, 67–77.
5. Small, B. L.; Brookhart, M. *J. Am. Chem. Soc.* **1998**, *120*, 7143–7144.
6. Small, B. L.; Brookhart, M.; Bennett, A. M. A. *J. Am. Chem. Soc.* **1998**, *120*, 4049–4050.
7. J. P. Britovsek, G.; C. Gibson, V.; J. McTavish, S.; A. Solan, G.; J. P. White, A.; J. Williams, D.; J. P. Britovsek, G.; S. Kimberley, B.; J. Maddox, P. *Chem. Commun.* **1998**, 849–850.
8. Britovsek, G. J. P.; Bruce, M.; Gibson, V. C.; Kimberley, B. S.; Maddox, P. J.; Mastroianni, S.; McTavish, S. J.; Redshaw, C.; Solan, G. A.; Strömberg, S.; White, A. J. P.; Williams, D. J. *J. Am. Chem. Soc.* **1999**, *121*, 8728–8740.
9. Gibson, V. C.; Redshaw, C.; Solan, G. A. *Chem. Rev.* **2007**, *107*, PMID: 17488059, 1745–1776.
10. Boudier, A.; Breuil, P.-A. R.; Magna, L.; Olivier-Bourbigou, H.; Braunstein, P. *Chem. Commun.* **2014**, *50*, 1398–1407.
11. Dudle, B.; Rajesh, K.; Blacque, O.; Berke, H. *J. Am. Chem. Soc.* **2011**, *133*, 8168–8178.
12. Jain, K. R.; Herrmann, W. A.; Kühn, F. E. *Coord. Chem. Rev.* **2008**, *252*, Chiral Catalysis, 556–568.
13. Kuninobu, Y.; Takai, K. *Chem. Rev.* **2011**, *111*, 1938–1953.
14. Kusama, H; Narasaka, K *Bull. Chem. Soc. Jpn.* **1995**, *68*, 2379–2383.
15. Nishiyama, Y.; Kakushou, F.; Sonoda, N. *Bull. Chem. Soc. Jpn.* **2000**, *73*, 2779–2782.
16. Kuninobu, Y.; Matsuki, T.; Takai, K. *J. Am. Chem. Soc.* **2009**, *131*, PMID: 19621953, 9914–9915.

17. Bolm, C.; Kesselgruber, M.; Hermanns, N.; Hildebrand, J. P.; Raabe, G. *Angew. Chem., Int. Ed.* **2001**, *40*, 1488–1490.

18. Zhao, W.-G.; Hua, R. *Tetrahedron* **2007**, *63*, 11803 –11808.

19. Kawata, A.; Kuninobu, Y.; Takai, K. *Chem. Lett.* **2009**, *38*, 836–837.

20. Hori, H.; Koike, K.; Takeuchi, K.; Ishitani, O. *Chem. Lett.* **2000**, *29*, 376–377.

21. Hua, R.; Tian, X. *J. Org. Chem.* **2004**, *69*, PMID: 15307759, 5782–5784.

22. Adams, R. D.; Falloon, S. B. *J. Am. Chem. Soc.* **1994**, *116*, 10540–10547.

23. Adams, R. D.; Huang, M.; Huang, W.; Queisser, J. A. *J. Am. Chem. Soc.* **1996**, *118*, 9442–9443.

24. Zhao, W.-G.; Hua, R. *Euro. J. Org. Chem.* **2006**, *2006*, 5495–5498.

25. Müller, T. E.; Grosche, M.; Herdtweck, E.; Pleier, A.-K.; Walter, E.; Yan, Y.-K. *Organometallics* **2000**, *19*, 170–183.

26. Bartholoma, M.; Valliant, J.; Maresca, K. P.; Babich, J.; Zubieta, J. *Chem. Commun.* **2009**, 493–512.

27. Schibli, R.; Schubiger, A. *Euro. J. Nuc. Med. Mol. Imaging* **2002**, *29*, 1529–1542.

28. Coogan, M.; Fernández-Moreira, V.; Kariuki, B.; Pope, S.; Thorp-Greenwood, F. *Angew. Chem., Int. Ed.* **2009**, *48*, 4965–4968.

29. Giordano, P. J.; Wrighton, M. S. *J. Am. Chem. Soc.* **1979**, *101*, 2888–2897.

30. Fredericks, S. M.; Luong, J. C.; Wrighton, M. S. *J. Am. Chem. Soc.* **1979**, *101*, 7415–7417.

31. Sacksteder, L.; Zipp, A. P.; Brown, E. A.; Streich, J.; Demas, J. N.; DeGraff, B. A. *Inorg. Chem.* **1990**, *29*, 4335–4340.

32. Caspar, J. V.; Meyer, T. J. *J. Phys. Chem.* **1983**, *87*, 952–957.

33. Yam, V. W.-W. *Chem. Commun.* **2001**, 789–796.

34. Feliz, M.; Rodriguez-Nieto, F.; Ruiz, G.; Wolcan, E. *J. Photochem. Photobiol., A* **1998**, *117*, 185 –192.

35. Ruiz, G.; Wolcan, E.; Féliz, M. *J. Photochem. Photobiol., A* **1996**, *101*, 119 –125.

36. Lin, R.; Fu, Y.; Brock, C. P.; Guarr, T. F. *Inorg. Chem.* **1992**, *31*, 4346–4353.

37. Hino, J. K.; Della Ciana, L.; Dressick, W. J.; Sullivan, B. P. *Inorg. Chem.* **1992**, *31*, 1072–1080.

38. Walters, K. A.; Kim, Y.-J.; Hupp, J. T. *Inorg. Chem.* **2002**, *41*, 2909–2919.

39. Striplin, D.; Crosby, G. *Coord. Chem. Rev.* **2001**, *211*, 163 –175.

40. Martin, T. A.; Ellul, C. E.; Mahon, M. F.; Warren, M. E.; Allan, D.; Whittlesey, M. K. *Organometallics* **2011**, *30*, 2200–2211.

41. Abel, E. W.; Wilkinson, G. *J. Chem. Soc.* **1959**, 1501–1505.
42. Kirkham, W. J.; Osborne, A. G.; Nyholm, R. S.; Stiddard, M. H. B. *J. Chem. Soc.* **1965**, 550–553.
43. Zingales, F.; Sartorelli, U.; Trovati, A. *Inorg. Chem.* **1967**, *6*, 1246–1248.
44. Gamelin, D. R.; George, M. W.; Glyn, P.; Grevels, F.-W.; Johnson, F. P. A.; Klotzbuecher, W.; Morrison, S. L.; Russell, G.; Schaffner, K.; Turner, J. J. *Inorg. Chem.* **1994**, *33*, 3246–3250.
45. Martí, A. A.; Mezei, G.; Maldonado, L.; Paralitici, G.; Raptis, R. G.; Colón, J. L. *Euro. J. Inorg. Chem.* **2005**, *2005*, 118–124.
46. Morse, D. L.; Wrighton, M. S. *J. Am. Chem. Soc.* **1976**, *98*, 3931–3934.
47. Ge, Q.; Corkery, T. C.; Humphrey, M. G.; Samoc, M.; Hor, T. S. A. *Dalton Trans.* **2009**, 6192–6200.
48. Giordano, P. J.; Fredericks, S. M.; Wrighton, M. S.; Morse, D. L. *J. Am. Chem. Soc.* **1978**, *100*, 2257–2259.
49. Granifo, J.; Bird, S. J.; Orrell, K. G.; Osborne, A. G.; Šik, V. *Inorg. Chem. Acta* **1999**, *295*, 56 –63.
50. Orrell, K. G.; Osborne, A. G.; Šik, V.; da Silva, M. W.; Hursthouse, M. B.; Hibbs, D. E.; Malik, K. A.; Vassilev, N. G. *J. Organomet. Chem.* **1997**, *538*, 171 –183.
51. Abel, E. W.; Dimitrov, V. S.; Long, N. J.; Orrell, K. G.; Osborne, A. G.; Pain, H. M.; Sik, V.; Hursthouse, M. B.; Mazid, M. A. *J. Chem. Soc., Dalton Trans.* **1993**, 597–603.
52. Potgieter, K.; Mayer, P.; Gerber, T.; Yumata, N.; Hosten, E.; Booysen, I.; Betz, R.; Ismail, M.; van Brecht, B. *Polyhedron* **2013**, *49*, 67 –73.
53. Gong, X.; Ng, P. K.; Chan, W. K. *Adv. Mater.* **1998**, *10*, 1337–1340.
54. Yu, T.; Tsang, D. P.-K.; Au, V. K.-M.; Lam, W. H.; Chan, M.-Y.; Yam, V. W.-W. *Chem.–Eur. J.* **2013**, *19*, 13418–13427.
55. Lo, K. K.-W.; Louie, M.-W.; Zhang, K. Y. *Coord. Chem. Rev.* **2010**, *254*, 18th International Symposium on the Photochemistry and Photophysics of Coordination Compounds Sapporo, 2009, 2603 –2622.
56. Lin, T.-P.; Chen, C.-Y.; Wen, Y.-S.; Sun, S.-S. *Inorg. Chem.* **2007**, *46*, 9201–9212.
57. Slone, R. V.; Yoon, D. I.; Calhoun, R. M.; Hupp, J. T. *J. Am. Chem. Soc.* **1995**, *117*, 11813–11814.
58. D. Beer, P.; Timoshenko, V.; Maestri, M.; Passaniti, P.; Balzani, V. *Chem. Commun.* **1999**, 1755–1756.
59. Beer, P. D.; Hayes, E. J. *Coord. Chem. Rev.* **2003**, *240*, 35 Years of Synthetic Anion Receptor Chemistry 1968-2003, 167 –189.

60. Amoroso, A. J.; Arthur, R. J.; Coogan, M. P.; Court, J. B.; Fernandez-Moreira, V.; Hayes, A. J.; Lloyd, D.; Millet, C.; Pope, S. J. A. *New J. Chem.* **2008**, *32*, 1097–1102.

61. Amoroso, A. J.; Coogan, M. P.; Dunne, J. E.; Fernandez-Moreira, V.; Hess, J. B.; Hayes, A. J.; Lloyd, D.; Millet, C.; Pope, S. J. A.; Williams, C. *Chem. Commun.* **2007**, 3066–3068.

62. Schutte, M.; Kemp, G.; Visser, H. G.; Roodt, A. *Inorg. Chem.* **2011**, *50*, 12486–12498.

63. Shestopalov, M. A.; Zubareva, K. E.; Khripko, O. P.; Khripko, Y. I.; Solovieva, A. O.; Kuratieva, N. V.; Mironov, Y. V.; Kitamura, N.; Fedorov, V. E.; Brylev, K. A. *Inorganic Chemistry* **0**, *0*, null.

64. Gimeno, M. C.; Fernandez-Moreira, V.; Marzo, I. *Chem. Sci.* **2014**, –.

65. Constable, E. C.; Thompson, A. M. W. C. *J. Chem. Soc., Dalton Trans.* **1992**, 3467–3475.

66. Hawecker, J.; Lehn, J.-M.; Ziessel, R. *J. Chem. Soc., Chem. Commun.* **1983**, 536–538.

67. Hawecker, J.; Lehn, J.-M.; Ziessel, R. *Helv. Chim. Acta* **1986**, *69*, 1990–2012.

68. Takeda, H.; Ishitani, O. *Coord. Chem. Rev.* **2010**, *254*, Inorganic Reaction Mechanisms A Tribute to Ralph Pearson on the occasion of his 90th birthday, 346 – 354.

69. Christensen, P.; Hamnett, A.; Muir, A. V. G.; Timney, J. A. *J. Chem. Soc., Dalton Trans.* **1992**, 1455–1463.

70. Sullivan, B. P.; Bolinger, C. M.; Conrad, D.; Vining, W. J.; Meyer, T. J. *J. Chem. Soc., Chem. Commun.* **1985**, 1414–1416.

71. Caulton, K. G. *Euro. J. Inorg. Chem.* **2012**, *2012*, 435–443.

72. Lyaskovskyy, V.; de Bruin, B. *ACS Catal.* **2012**, *2*, 270–279.

73. Jurca, T.; Chen, W.-C.; Michel, S.; Korobkov, I.; Ong, T.-G.; Richeson, D. S. *Chem.–Eur. J.* **2013**, *19*, 4278–4286.

74. Juris, A.; Campagna, S.; Bidd, I.; Lehn, J. M.; Ziessel, R. *Inorg. Chem.* **1988**, *27*, 4007–4011.

75. Black, D. R.; Hightower, S. E. *Inorg. Chem. Commun.* **2012**, *24*, 16 –19.

76. Song, C. *Catal. Today* **2006**, *115*, Proceedings of the 8th International Conference on Carbon Dioxide Utilization Dedicated to Professor Michele Aresta, 2 –32.

77. Matthews, H. D.; Gillett, N. P.; Stott, P. A.; Zickfeld, K. *Nature* **June 2009**, *459*, 829–832.

78. Meinshausen, M.; Meinshausen, N.; Hare, W.; Raper, S. C. B.; Frieler, K.; Knutti, R.; Frame, D. J.; Allen, M. R. *Nature* **Apr. 2009**, *458*, 1158–1162.
79. Neuhoff, K. *Oxford Rev. Econ. Policy* **2005**, *21*, 88–110.
80. Pera-Titus, M. *Chem. Rev.* **2014**, *114*, 1413–1492.
81. Kadantsev, E. S.; Boyd, P. G.; Daff, T. D.; Woo, T. K. *J. Phys. Chem. Lett.* **2013**, *4*, 3056–3061.
82. Iremonger, S. S.; Liang, J.; Vaidhyanathan, R.; Martens, I.; Shimizu, G. K. H.; Daff Thomas, D.; Aghaji, M. Z.; Yeganegi, S.; Woo, T. K. *J. Am. Chem. Soc.* **2011**, *133*, 20048–20051.
83. Leitner, W. *Coord. Chem. Rev.* **1996**, *153*, 257 –284.
84. Olah, G. A.; Goeppert, A.; Prakash, G. K. S., *Beyond Oil and Gas: The Methanol Economy*, 2nd; Wiley: 2009.
85. Kang, P.; Cheng, C.; Chen, Z.; Schauer, C. K.; Meyer, T. J.; Brookhart, M. *J. Am. Chem. Soc.* **2012**, *134*, 5500–5503.
86. Schwarz, H. A.; Dodson, R. W. *J. Phys. Chem.* **1989**, *93*, 409–414.
87. Morris, A. J.; Meyer, G. J.; Fujita, E. *Acc. Chem. Res.* **2009**, *42*, PMID: 19928829, 1983–1994.
88. Arakawa, H. et al. *Chem. Rev.* **2001**, *101*, PMID: 11709862, 953–996.
89. Li, W. In *Advances in CO¡sub¿2¡/sub¿ Conversion and Utilization*; ACS Symposium Series, Vol. 1056; American Chemical Society: 2010; Chapter 5, pp 55–76.
90. Inoue, T.; Fujishima, A.; Konishi, S.; Honda, K. *Nature* **Feb. 1979**, *277*, 637–638.
91. Lim, H.-K.; Shin, H.; Goddard, W. A.; Hwang, Y. J.; Min, B. K.; Kim, H. *J. Am. Chem. Soc.* **2014**, *136*, 11355–11361.
92. Fisher, B. J.; Eisenberg, R. *J. Am. Chem. Soc.* **1980**, *102*, 7361–7363.
93. Tinnemans, A. H. A.; Koster, T. P. M.; Thewissen, D. H. M. W.; Mackor, A. *Recueil des Travaux Chimiques des Pays-Bas* **1984**, *103*, 288–295.
94. Beley, M.; Collin, J. P.; Ruppert, R.; Sauvage, J. P. *J. Am. Chem. Soc.* **1986**, *108*, 7461–7467.
95. Simon-Manso, E.; Kubiak, C. P. *Organometallics* **2004**, *24*, 96–102.
96. Fujita, E.; Haff, J.; Sanzenbacher, R.; Elias, H. *Inorg. Chem.* **1994**, *33*, 4627–4628.
97. Fujita, E.; Creutz, C.; Sutin, N.; Brunschwig, B. S. *Inorg. Chem.* **1993**, *32*, 2657–2662.
98. Kimura, E.; Wada, S.; Shionoya, M.; Okazaki, Y. *Inorg. Chem.* **1994**, *33*, 770–778.
99. Dhanasekaran, T.; Grodkowski, J.; Neta, P.; Hambright, P.; Fujita, E. *J. Phys. Chem. A* **1999**, *103*, 7742–7748.

100. Lacy, D. C.; McCrory, C. C. L.; Peters, J. C. *Inorg. Chem.* **2014**, *53*, 4980–4988.

101. Bourrez, M.; Molton, F.; Chardon-Noblat, S.; Deronzier, A. *Angew. Chem., Int. Ed.* **2011**, *50*, 9903–9906.

102. Sampson, M. D.; Nguyen, A. D.; Grice, K. A.; Moore, C. E.; Rheingold, A. L.; Kubiak, C. P. *J. Am. Chem. Soc.* **2014**, *136*, 5460–5471.

103. Zeng, Q.; Tory, J.; Hartl, F. *Organometallics* **0**, *0*, null.

104. Roy, S. C.; Varghese, O. K.; Paulose, M.; Grimes, C. A. *ACS Nano* **2010**, *4*, PMID: 20141175, 1259–1278.

105. Asatani, T.; Nakagawa, Y.; Funada, Y.; Sawa, S.; Takeda, H.; Morimoto, T.; Koike, K.; Ishitani, O. *Inorg. Chem.* **2014**, *53*, 7170–7180.

106. Schneider, J.; Vuong, K. Q.; Calladine, J. A.; Sun, X.-Z.; Whitwood, A. C.; George, M. W.; Perutz, R. N. *Inorg. Chem.* **2011**, *50*, 11877–11889.

107. Ishida, H.; Tanaka, K.; Tanaka, T. *Organometallics* **1987**, *6*, 181–186.

108. Maidan, R.; Willner, I. *J. Am. Chem. Soc.* **1986**, *108*, 8100–8101.

109. Ishida, H.; Terada, T.; Tanaka, K.; Tanaka, T. *Inorg. Chem.* **1990**, *29*, 905–911.

110. Kitamura, N.; Tazuke, S. *Chem. Lett.* **1983**, *12*, 1109–1112.

111. Tanaka, K.; Ooyama, D. *Coord. Chem. Rev.* **2002**, *226*, 211 –218.

112. Doherty, M. D.; Grills, D. C.; Fujita, E. *Inorg. Chem.* **2009**, *48*, 1796–1798.

113. Doherty, M. D.; Grills, D. C.; Muckerman, J. T.; Polyansky, D. E.; Fujita, E. *Coord. Chem. Rev.* **2010**, *254*, 18th International Symposium on the Photochemistry and Photophysics of Coordination Compounds Sapporo, 2009, 2472 –2482.

114. Tamaki, Y.; Koike, K.; Morimoto, T.; Yamazaki, Y.; Ishitani, O. *Inorg. Chem.* **2013**, *52*, 11902–11909.

115. Sato, S.; Morikawa, T.; Kajino, T.; Ishitani, O. *Angew. Chem., Int. Ed.* **2013**, *52*, 988–992.

116. Reithmeier, R. O.; Meister, S.; Rieger, B.; Siebel, A.; Tschurl, M.; Heiz, U.; Herdtweck, E. *Dalton Trans.* **2014**, –.

117. Hori, H.; Johnson, F. P.; Koike, K.; Ishitani, O.; Ibusuki, T. *J. Photochem. Photobiol., A* **1996**, *96*, 171 –174.

118. Takeda, H.; Koike, K.; Inoue, H.; Ishitani, O. *J. Am. Chem. Soc.* **2008**, *130*, 2023–2031.

119. Grills, D. C.; Fujita, E. *J. Phys. Chem. Lett.* **2010**, *1*, 2709–2718.

120. Windle, C. D.; Perutz, R. N. *Coord. Chem. Rev.* **2012**, *256*, Solar Fuels- by invitation only, 2562 –2570.

121. Shavaleev, N. M.; Barbieri, A.; Bell, Z. R.; Ward, M. D.; Barigelletti, F. *New J. Chem.* **2004**, *28*, 398–405.

122. Kutal, C.; Weber, M. A.; Ferraudi, G.; Geiger, D. *Organometallics* **1985**, *4*, 2161–2166.

123. Larsen, C. B.; van der Salm, H.; Clark, C. A.; Elliott, A. B. S.; Fraser, M. G.; Horvath, R.; Lucas, N. T.; Sun, X.-Z.; George, M. W.; Gordon, K. C. *Inorg. Chem.* **2014**, *53*, 1339–1354.

124. Russell, S. K.; Darmon, J. M.; Lobkovsky, E.; Chirik, P. J. *Inorg. Chem.* **2010**, *49*, PMID: 20143847, 2782–2792.

125. Tondreau, A. M.; Atienza, C. C. H.; Weller, K. J.; Nye, S. A.; Lewis, K. M.; Delis, J. G. P.; Chirik, P. J. *Science* **2012**, *335*, 567–570.

126. SciFinder. Chemical Abstracts Services, a division of the American Chemical Society.

127. Buckingham, D.; Dwyer, F.; Goodwin, H.; Sargeson, A. *Aust. J. Chem.* **1964**, *17*, 315–324.

128. Jurca, T. Charting New Territory in Bis(imino)pyridine Coordination Chemistry., PhD Thesis, University of Ottawa, 2012.

129. Morimoto, T.; Nakajima, T.; Sawa, S.; Nakanishi, R.; Imori, D.; Ishitani, O. *J. Am. Chem. Soc.* **2013**, *135*, 16825–16828.

130. Anderson, P. A.; Keene, F. R.; Horn, E.; Tiekink, E. R. T. *Appl. Organomet. Chem.* **1990**, *4*, 523–533.

131. Civitello, E. R.; Dragovich, P. S.; Karpishin, T. B.; Novick, S. G.; Bierach, G.; O'Connell, J. F.; Westmoreland, T. D. *Inorg. Chem.* **1993**, *32*, 237–241.

132. Kurz, P.; Probst, B.; Spingler, B.; Alberto, R. *Euro. J. Inorg. Chem.* **2006**, *2006*, 2966–2974.

133. Becke, A. D. *J. Chem. Phys.* **1993**, *98*, 5648–5652.

134. Lee, C.; Yang, W.; Parr, R. G. *Phys. Rev. B* **1988**, *37*, 785–789.

135. Frisch, M. J. et al. Gaussian 09 Revision D.01., Gaussian Inc. Wallingford CT 2009.

136. Hay, P. J.; Wadt, W. R. *J. Chem. Phys.* **1985**, *82*, 299–310.

137. Schäfer, A.; Huber, C.; Ahlrichs, R. *J. Chem. Phys.* **1994**, *100*, 5829–5835.

138. Zhang, I. Y.; Wu, J.; Xu, X. *Chem. Commun.* **2010**, *46*, 3057–3070.

139. Zhao, Y.; Truhlar, D. G. *Accounts of Chemical Research* **2008**, *41*, 157–167.

140. Tomasi, J.; Mennucci, B.; Cammi, R. *Chem. Rev.* **2005**, *105*, 2999–3094.

141. Scalmani, G.; Frisch, M. J.; Mennucci, B.; Tomasi, J.; Cammi, R.; Barone, V. *J. Chem. Phys.* **2006**, *124* 094107, –.

142. Compain, J.-D.; Bourrez, M.; Haukka, M.; Deronzier, A.; Chardon-Noblat, S. *Chem. Commun.* **2014**, *50*, 2539–2542.

143. Allen, F. H. *Acta Crystallogr. Sect. B* **2002**, *58*, 380–388.

144. Andersson, M. P.; Uvdal, P. *The Journal of Physical Chemistry A* **2005**, *109*, PMID: 16833612, 2937–2941.

145. Portenkirchner, E.; Kianfar, E.; Sariciftci, N. S.; Knör, G. *ChemSusChem* **2014**, *7*, 1347–1351.

146. Rossenaar, B. D.; Hartl, F.; Stufkens, D. J. *Inorg. Chem.* **1996**, *35*, 6194–6203.

147. Hayashi, Y.; Kita, S.; Brunschwig, B. S.; Fujita, E. *J. Am. Chem. Soc.* **2003**, *125*, PMID: 14505419, 11976–11987.

148. Agarwal, J.; Johnson, R. P.; Li, G. *J. Phys. Chem. A* **2011**, *115*, 2877–2881.

149. Agarwal, J.; Sanders, B. C.; Fujita, E.; Schaefer III, H. F.; Harrop, T. C.; Muckerman, J. T. *Chem. Commun.* **2012**, *48*, 6797–6799.

150. Agarwal, J.; Fujita, E.; Schaefer, H. F.; Muckerman, J. T. *J. Am. Chem. Soc.* **2012**, *134*, 5180–5186.

151. Keith, J. A.; Grice, K. A.; Kubiak, C. P.; Carter, E. A. *J. Am. Chem. Soc.* **2013**, *135*, 15823–15829.

152. Grills, D. C.; Matsubara, Y.; Kuwahara, Y.; Golisz, S. R.; Kurtz, D. A.; Mello, B. A. *J. Phys. Chem. Lett.* **2014**, *5*, 2033–2038.

153. Martin, R. B.; Lissfelt, J. A. *J. Am. Chem. Soc.* **1956**, *78*, 938–940.

154. Zink, J. I. *Coord. Chem. Rev.* **2001**, *211*, 69 –96.

155. Johnson, F. P. A.; George, M. W.; Hartl, F.; Turner, J. J. *Organometallics* **1996**, *15*, 3374–3387.

156. Koike, K.; Okoshi, N.; Hori, H.; Takeuchi, K.; Ishitani, O.; Tsubaki, H.; Clark, I. P.; George, M. W.; Johnson, F. P. A.; Turner, J. J. *J. Am. Chem. Soc.* **2002**, *124*, 11448–11455.

157. Gibson, D. H.; Yin, X.; He, H.; Mashuta, M. S. *Organometallics* **2003**, *22*, 337–346.

158. Smieja, J. M.; Benson, E. E.; Kumar, B.; Grice, K. A.; Seu, C. S.; Miller, A. J. M.; Mayer, J. M.; Kubiak, C. P. *Proc. Natl. Acad. Sci. U. S. A.* **2012**, *109*, 15646–15650.

159. Machan, C. W.; Sampson, M. D.; Chabolla, S. A.; Dang, T.; Kubiak, C. P. *Organometallics* **2014**, *Accepted Article*, DOI: 10.1021/om500044a.

160. Kou, Y.; Nabetani, Y.; Masui, D.; Shimada, T.; Takagi, S.; Tachibana, H.; Inoue, H. *J. Am. Chem. Soc.* **2014**, *136*, 6021–6030.

161. Hawecker, J.; Lehn, J.-M.; Ziessel, R. *J. Chem. Soc., Chem. Commun.* **1984**, 328–330.

162. Kalyanasundaram, K.; Kiwi, J.; Grätzel, M. *Helv. Chim. Acta* **1978**, *61*, 2720–2730.

163. TURBOMOLE V6.5, a development of University of Karlsruhe and Forschungszentrum Karlsruhe GmbH., available from www.turbomole-gmbh.com, 2013.

164. Ahlrichs, R.; Bär, M.; Häser, M.; Horn, H.; Kölmel, C. *Chem. Phys. Lett.* **1989**, *162*, 165 –169.

165. Tao, J.; Perdew, J. P.; Staroverov, V. N.; Scuseria, G. E. *Phys. Rev. Lett.* **2003**, *91*, 146401.

166. Weigend, F.; Ahlrichs, R. *Phys. Chem. Chem. Phys.* **2005**, *7*, 3297–3305.

167. Haase, F.; Ahlrichs, R. *J. Comput. Chem.* **1993**, *14*, 907–912.

168. Treutler, O.; Ahlrichs, R. *J. Chem. Phys.* **1995**, *102*, 346–354.

169. Eichkorn, K.; Weigend, F.; Treutler, O.; Ahlrichs, R. *Theor. Chem. Acc.* **1997**, *97*, 119–124.

170. Eichkorn, K; Treutler, O; Öhm, H; Häser, M; Ahlrichs, R *Chem. Phys. Lett.* **1995**, *242*, 652 –660.

171. Sierka, M.; Hogekamp, A.; Ahlrichs, R. *J. Chem. Phys.* **2003**, *118*, 9136–9148.

172. Deglmann, P.; May, K.; Furche, F.; Ahlrichs, R. *Chem. Phys. Lett.* **2004**, *384*, 103 –107.

173. Weigend, F. *Phys. Chem. Chem. Phys.* **2002**, *4*, 4285–4291.

174. Von Arnim, M.; Ahlrichs, R. *J. Comput. Chem.* **1998**, *19*, 1746–1757.

175. Ahlrichs, R. *Phys. Chem. Chem. Phys.* **2004**, *6*, 5119–5121.

176. Grimme, S.; Antony, J.; Ehrlich, S.; Krieg, H. *J. Chem. Phys.* **2010**, *132* 154104, –.

177. Deglmann, P.; Furche, F.; Ahlrichs, R. *Chem. Phys. Lett.* **2002**, *362*, 511 –518.

178. Grimme, S.; Furche, F.; Ahlrichs, R. *Chem. Phys. Lett.* **2002**, *361*, 321 –328.

179. Klamt, A.; Schuurmann, G. *J. Chem. Soc., Perkin Trans. 2* **1993**, 799–805.

180. Shaver, R. J.; Rillema, D. P. *Inorg. Chem.* **1992**, *31*, 4101–4107.

181. Gibson, D. H.; Yin, X. *J. Am. Chem. Soc.* **1998**, *120*, 11200–11201.

182. H. Gibson, D.; Yin, X. *Chem. Commun.* **1999**, 1411–1412.

183. Fujita, E.; Muckerman, J. T. *Inorg. Chem.* **2004**, *43*, PMID: 15554628, 7636–7647.

184. Bokarev, S. I.; Hollmann, D.; Pazidis, A.; Neubauer, A.; Radnik, J.; Kuhn, O.; Lochbrunner, S.; Junge, H.; Beller, M.; Bruckner, A. *Phys. Chem. Chem. Phys.* **2014**, *16*, 4789–4796.

185. Chisholm, M. H.; Huffman, J. C.; Rothwell, I. P.; Bradley, P. G.; Kress, N.; Woodruff, W. H. *J. Am. Chem. Soc.* **1981**, *103*, 4945–4947.

186. Castella-Ventura, M.; Kassab, E.; Buntinx, G.; Poizat, O. *Phys. Chem. Chem. Phys.* **2000**, *2*, 4682–4689.

187. Gore-Randall, E.; Irwin, M.; Denning, M. S.; Goicoechea, J. M. *Inorg. Chem.* **2009**, *48*, PMID: 19673484, 8304–8316.

188. Irwin, M.; Jenkins, R. K.; Denning, M. S.; Krämer, T.; Grandjean, F.; Long, G. J.; Herchel, R.; McGrady, J. E.; Goicoechea, J. M. *Inorg. Chem.* **2010**, *49*, 6160–6171.

189. Lukehart, C.; Zeile, J. V. *J. Organomet. Chem.* **1977**, *140*, 309 –316.

190. *CRC Handbook of Chemistry and Physics*, 79th Edition; Lide, D. R., Ed.; CRC Press LLC: Boca Raton, FL, 1998.

191. Sullivan, B. P.; Meyer, T. J. *J. Chem. Soc., Chem. Commun.* **1984**, 1244–1245.

192. Sullivan, B. P.; Meyer, T. J. *Organometallics* **1986**, *5*, 1500–1502.

193. Creutz, C.; Chou, M. H. *J. Am. Chem. Soc.* **2007**, *129*, 10108–10109.

194. Lee, H.-J.; Lloyd, M. D.; Harlos, K.; Clifton, I. J.; Baldwin, J. E.; Schofield, C. J. *J. Mol. Biol.* **2001**, *308*, 937 –948.

195. Mauser, H.; King, W. A.; Gready, J. E.; Andrews, T. J. *J. Am. Chem. Soc.* **2001**, *123*, PMID: 11686683, 10821–10829.

196. Souter, P. F.; Andrews, L. *J. Am. Chem. Soc.* **1997**, *119*, 7350–7360.

197. Castro-Rodriguez, I.; Nakai, H.; Zakharov, L. N.; Rheingold, A. L.; Meyer, K. *Science* **2004**, *305*, 1757–1759.

198. Cokoja, M.; Bruckmeier, C.; Rieger, B.; Herrmann, W. A.; Kühn, F. E. *Angew. Chem., Int. Ed.* **2011**, *50*, 8510–8537.

199. Gibson, D. H. *Chem. Rev.* **1996**, *96*, 2063–2096.

200. Van Rossum; Barry Warsaw; Nick Coghlan, G. Style Guide for Python Code., 2132f8d8bcb4; Python.org, 2013.

201. Goodger, D.; van Rossum, G. Docstring Conventions., 4b5a1100c7af; Python.org, 2001.

202. Bulsink, P. TurboControl v1.1.0., `http://github.com/pbulsink/turbocontrol`.

203. Skripnikov, L. Chemissian, a computer program to analye and visualize quantum-chemical calculations., `http://chemissian.com`.

204. APEX Software Suite v.2010., Bruker AXS: Madison, WI, 2005.

205. Blessing, R. H. *Acta Crystallogr. Sect. A* **1995**, *51*, 33–38.

206. Sheldrick, G. Cell_Now., Bruker AXS: Madison, WI, 2004.

207. Sheldrick, G. M. *Acta Crystallogr. Sect. A* **2008**, *64*, 112–122.

208. Spurrier, N. Pexpect, version 3.2., `http://pexpect.readthedocs.org/en/latest/index.html`.

209. Open Babel Package, version 2.3.1., `http://openbabel.org`.

210. O'Boyle, N. M.; Banck, M; James, C. A.; Morley, C; Vandermeersch, T; Hutchison, G. R. *J. Cheminf.* **2011**, *3*, 33.